Processing and release of the maize phytocytokine Zip1

Maurice Koenig[1], Zarah Sorger[1], Melissa Mantz[2,3], Andreas Perrar[2], Pitter F. Huesgen[2,3,4], Simon Stael[5], Johana Misas Villamil[1#], Gunther Doehlemann[1#]

[1] Institute for Plant Sciences and Cluster of Excellence on Plant Sciences (CEPLAS), University of Cologne, Cologne, Germany
[2] Central Institute for Engineering, Electronics and Analytics, ZEA-3, Forschungzentrum Jülich
[3] Institute of Biology II, University of Freiburg, Freiburg, Germany
[4] CIBSS-Centre for Integrative Biological Signaling Studies, University of Freiburg, Freiburg, Germany
[5] Department of Molecular Sciences, Uppsala BioCenter, Swedish University of Agricultural Sciences and Linnean Center for Plant Biology, Uppsala, Sweden

[#]Corresponding authors: jmisas@uni-koeln.de, g.doehlemann@uni-koeln.de

---

Keywords: Zip1, phytocytokine, apoplastic immunity, metacaspase, PLCPs

Abstract

Phytocytokines are peptide signaling molecules in plant immunity. Extracellular phytocytokines and their cognate membrane-receptors have been described in various species; however, processing and release of these signals remains largely unknown. The *Zea mays* immune peptide 1 (Zip1) is a maize-specific phytocytokine, which is associated to the salicylic acid (SA) signaling pathway. Zip1 resides central in its precursor PROZIP1, thus C- and N-terminal cleavage is required to release bioactive Zip1 peptide. Two apoplastic maize PLCPs, CP1 and CP2, were previously shown to cleave PROZIP1. We investigated the localization and processing steps of PROZIP1 leading to Zip1 release and found that PROZIP1 undergoes processing in the endoplasmic reticulum (ER) and cytoplasm, where the N-terminal PROZIP1 is cleaved. C-terminal PROZIP1 translocates to the apoplast via an unconventional secretion pathway, likely involving exocyst-positive organelles (EXPO). The combination of antibody detection, protease cleavage assays and mass spectrometry provided evidence for a proteolytic cascade, in which intracellular processing of PROZIP1 is executed by the calcium-dependent metacaspases ZmMC9 through arginine-dependent cleavage. After secretion, C-terminal PROZIP1 is processed by apoplastic PLCPs, which release, but also degrade the Zip1 peptide. Together, these findings reveal a two-step mechanism of phytocytokine processing, translocation, activation and clearance.

Introduction

Plant signalling peptides, named phytocytokines, are secondary endogenous danger signals, which are actively released upon damage and environmental stimuli and play roles in growth, development, and immunity. The term phytocytokine is based on their shared features with metazoan cytokines (Luo *et al*., 2012; Gust *et al*., 2017; Hou *et al.*, 2019). Wounding, pathogen infection or the perception of microbe-associated molecular patterns (MAMPs) induce the production of phytocytokines, which act as immunomodulatory peptides (Hou *et al*., 2021; Yamaguchi & Kawasaki, 2021; Koenig *et al*., 2023). Phytocytokines can fulfil various functions. For instance, *Zea mays* immune peptide 1 (Zip1), plant elicitor peptides (Peps), PAMP-induced peptides (PIPs), serine-rich endogenous peptides (SCOOPs), GRIM REAPER (GRI) and GmSubPeps are considered as amplifiers of extracellular immune responses and are mainly associated to salicylic acid-mediated signalling (Ziemann *et al*., 2018;

Zelman *et al*., 2023; Segonzac *et al*., 2019; Hou *et al*., 2021; Wrzaczek *et al*., 2015). Rapid alkalization factors (RALFs) are involved in growth and development while cellular processes related to immunity are supressed (Bedinger *et al*., 2010; Liu *et al.,* 2024).

Phytocytokines are classified as secreted or non-secreted based on whether their precursors have a signal peptide (Matsubayashi *et al*., 2014). Non-secreted phytocytokines, such as Systemins, PEP1, Zip1, and GmPEPs, lack a signal peptide for extracellular localization. In contrast, secreted phytocytokines including hydroxyproline-rich systemin (HypSys), PIP1/2, SCOOP12, phytosulfokines (PSKs), plant peptides containing sulfated tyrosine 1 (PSY1), inflorescence deficient in abscission (IDA) and its homolog IDA-LIKE 6 (IDL6), root meristem growth factors (RGFs)/GOLVENs (GLVs) and RALFs are derived from precursors that contain an extracellular localization signal. Tanaka and Heil (2021) classify into constitutive DAMPs (cDAMPs), like ATP, histones, and self-DNA, which perform conserved roles, but signal damage only when displaced or fragmented, and inducible DAMPs (iDAMPs), such as immunomodulatory peptides or phytocytokines, which function solely as damage-induced signals. The coevolution of these signals with their receptors likely linked damage detection to conserved immune pathways (Tanaka and Heil, 2021).

Phytocytokine-mediated processes are dynamic and highly adaptable, enabling a precisely coordinated and timely immune response. Phytocytokines can be transcriptionally induced, undergo maturation by proteolytic cleavage (processing) and can carry posttranslational modifications prior their release to the plant's apoplast. The processing of phytocytokine precursors is a mechanistically complex phenomenon, as multiple proteases and various cell compartments can be involved (Stührwohldt *et al*., 2020; Hou *et al*., 2021; Liu *et al*., 2022, Koenig *et al*., 2025). As a result, despite the great importance of phytocytokines as initiators of danger-triggered immunity (DTI) (Del Corpo *et al*., 2024), the mechanism of phytocytokine release remains poorly characterized. One of the most mechanistically best understood phytocytokines is Systemin (Sys), the first identified plant peptide hormone discovered in *Solanum lycopersicum* (Pearce *et al*., 1991). Its active form consists of 18 amino acids and is induced in response to wounding. PROSys processing occurs intracellularly where a phytaspase cleaves two Asp residues of the 200-amino acid precursor to release the intermediate Leu-Systemin. For its bioactivity, the N-terminal

leucine must be removed, likely by a Leu aminopeptidase (Beloshistov *et al*., 2018). Systemin is recognized by the receptor-like kinase SYR1, triggering early and late responses including an oxidative burst, ethylene production and formation of the jasmonic acid (JA) intermediate 12-oxo-phytodienoic acid (OPDA) that controls late responses such as expression of defense-related genes and the biosynthesis of secondary metabolites (Felix and Boller, 1995; Ryan *et al*., 2000; Wang *et al*., 2018).

The identification of proteases involved in phytocytokine release is a challenging process, and as a result, the proteases responsible for releasing bioactive phytocytokines are often unknown. The most abundant proteases in the plant apoplast, papain-like cysteine proteases (PLCPs) and serine proteases (subtilases) (Sueldo *et al*., 2014; Grosse-Holz *et al*., 2018), have also been found to be involved in phytocytokine release. The apoplastic PLCPs, CP1 and CP2 were found to be involved in the processing of apoplastic Zip1 from its precursor PROZIP1 (Ziemann *et al*.,2018). In addition to CP1 and CP2, the Xylem Cysteine Peptidase 1 (XCP1) has been identified as the protease responsible for processing PR1 in Arabidopsis, thereby facilitating the release of CAPE9, which belongs to the CAPE phytocytokines (Chen *et al.*, 2023). Additionally, *Triticum aestivum* RD21, an orthologue of CP1, has been shown to release Wip1 from its precursor, thus conferring wheat resistance to wheat yellow mosaic virus (Liu *et al*., 2023). Besides, subtilases (SBTs) have been identified as proteases releasing MAMPs and phytocytokines. Subtilases are involved in general proteolysis but can also offer high specificity as processing proteases (Schardon *et al*., 2016). Phytaspases are a class of subtilases releasing Systemin (Beloshistov *et al*., 2018). SBT1.1, SBT3.8, and SBT6.1 have been identified as the processing proteases involved in the release of phytosulfokine 1 (PSK1), plant peptides containing tyrosine sulfation (PSYs), CLAVATA3/ENDOSPERM SURROUNDING REGION-RELATED-like (CLEL) peptides and GOLVEN1 (GLV1) (Srivastava *et al*., 2008; Stührwohldt *et al*., 2021; Stührwohldt *et al*., 2020; Ghorbani *et al*., 2016). Lastly, the Site-1 protease (S1P), another, has been identified as the processing protease of ProRALF23 in Arabidopsis (Srivastava *et al*., 2009).

Metacaspases (MCAs), which are predominantly intracellularly localized, have also been implicated in phytocytokine processing and release. In *A. thaliana,* Pep1 (AtPep1) is released from its precursor AtPROPEP1, by METACASPASE 4 (AtMC4/AtMCA-IIa), which is activated via an increase in calcium influx (Ca^{2+}) upon damage. AtMC4 cleaves AtPROPEP1 at a specific arginine residue (R^{69}) in its

C-terminal region, resulting in the maturation and release of AtPep1. Perception of AtPep1 subsequently activates defense mechanisms (Hander *et al*., 2019). Similarly, Arabidopsis METACASPASE 9 (AtMC9/AtMCA-IIf) processes the phytocytokine precursor GRIp, releasing GRI through cleavage at the arginine (R^{67}) and lysine (K^{78}) residues, which are characteristic of metacaspase activity (Tsiatsiani *et al*., 2013; Wrzaczek *et al*., 2015; Vercammen *et al*., 2004). Frequently, the subcellular localization of phytocytokine precursors and the mechanism by which phytocytokines reach the extracellular space remain unknown.

Zip1, a maize-specific phytocytokine, enhances salicylic acid (SA)-mediated immunity and activates PLCPs, central hubs in plant defense, ultimately promoting resistance to the biotrophic fungus *Ustilago maydis* (Ziemann *et al*., 2018; Misas Villamil *et al*., 2016). Here, we investigated the subcellular localization and maturation of PROZIP1, which follows a two-step mechanism: an intracellular maturation step preceding the exocytosis-mediated release of a C-terminal Zip1containing fragment into the apoplast, followed by a second apoplastic cleavage for the timely regulated release and clearance of the bioactive Zip1.

Results

Zip1 triggers *Prozip1* expression and specific transcriptomic responses

Previous work showed that Zip1-induced gene expression strongly overlaps with the SA response at 24 hours post-treatment (Ziemann *et al*., 2018). However, in the same work, the expression of *Prozip1* could not be detected 24 hours after SA treatment. We therefore hypothesized that transcriptional regulation of *Prozip1* might occur earlier and conducted a time course experiment after treatments with either SA or Zip1. Maize leaves were treated with either SA, Zip1 peptide or a mock solution and the expression of *Prozip1* was evaluated after three, six and nine hours after mock, SA and Zip1 treatments, respectively. The responsiveness to SA- and Zip1-treatments was confirmed by the upregulation of *ZmWrky65* at 3 hpi (Koenig & Moser *et al*., 2023) (Fig. S1A). *Prozip1* showed a significant upregulation three and nine hours after SA- and six and nine hours after Zip1-treatment, respectively (Fig. 1A). In contrast, mock samples did not induce the expression of *Prozip1* at any tested time point (Fig. 1A) indicating that *Prozip1* expression is regulated by SA and Zip1. Next, we performed RNA sequencing (RNA-seq) at 6 hpi to gain specific insights into the transcriptional processes taking place when Zip1-signaling is being initiated (Table

S1). A principal component analysis (PCA) showed distinct grouping of mock, SA, and Zip1 (Fig. S1B), suggesting significant disparities in gene expression. In total, 1188 genes were differentially expressed in response to SA and Zip1 treatments compared to the mock control, whereas only 52 genes were commonly regulated by both treatments (Fig. 1B). SA treatment led to the upregulation of 479 genes (115 genes downregulated), while in response to Zip1 treatment, only 111 genes were induced, but 483 genes were downregulated. To further characterize differentially expressed genes (DEGs) and identify shared transcriptional patterns, genes were categorized based on their associated Gene Ontology (GO) terms, with particular attention given to immunity-related categories. SA treatment induced the expression of genes attributed to general immunity, hormone signaling, cytochrome P450s (CYPs), glutathione-S-transferases (GSTs), proteases, receptors and WRKY transcription factors (Fig. 1C). Zip1 treatment also upregulated genes in all these categories except for GSTs, which were exclusively induced by SA. However, the induced gene sets largely differed between treatments. Notably, Zip1 upregulated a higher number of receptor genes.

Both PLCPs, CP1 (Zm00001eb066830) and CP2 (Zm00001eb314220), were upregulated by Zip1 and SA, respectively. This is particularly remarkable, because these enzymes have been previously proposed to mediate apoplastic Zip1 release (Ziemann *et al*., 2018) (Fig. S1C). Furthermore, genes associated with calcium (Ca^{2+}) signaling and the microsomal compartment were overrepresented following Zip1-treatment (Fig. 1C). Several Ca^{2+}-sensors and -transporters were transcriptionally upregulated in response to Zip1, consistent with their established roles in plant immunity (Jiang *et al*., 2023; Wang *et al*., 2024) (Fig. S1D). Microsome-related genes included those implicated in the regulation of endocytosis, vesicular trafficking, and secretion (Fig. S1D). This reflects a targeted fine-tuning of immune responses which is characteristic of phytocytokines as immune modulators (Hou *et al*., 2021; Rzemieniewski & Stegmann, 2022; Koenig *et al*., 2023; Jian *et al*., 2024).

In summary, transcriptome analysis revealed distinct transcriptional responses between Zip1 and SA at six hours after treatment. Moreover, Zip1-specific gene regulation reflects intracellular processes including Ca^{2+}-signaling and microsome/membrane trafficking and eventually proteases responsible for

processing and release of PROZIP1/Zip1. These findings suggest the involvement of an intracellular mechanism in PROZIP1 maturation

PROZIP1 localizes intracellularly and is ER-associated

Following the findings of the transcriptome analysis that early Zip1 signaling involves modulation of specific intracellular processes, we set up to investigate intracellular localization of PROZIP1. To this end, we generated overexpression constructs of PROZIP1 carrying C-terminal fluorescent tags. The PROZIP1 fusion proteins were expressed in maize protoplasts for microscopic analysis. Upon expression in *Z. mays* protoplasts, PROZIP1 localized intracellularly showing signals in the periphery of the nuclei and cytoplasm, compared to the NLS-mCherry construct, which showed a nuclear localization (Fig. S2A). To determine whether PROZIP1 and its cleavage site mutant (PROZIP1$^{CS\text{-}mut}$; Ziemann *et al*., 2018) differ in localization, maize protoplasts were transfected. PROZIP1-GFP and PROZIP1$^{CS\text{-}mut}$-GFP localized in the protoplast's nuclear periphery and cytoplasm (Fig. 2A). The overlay of GFP and mCherry showed partially overlapping signals of nuclear-localized mCherry with PROZIP1-GFP and PROZIP1$^{CS\text{-}mut}$-GFP. In addition, GFP fluorescence was observed in cytoplasmic threads, indicating that PROZIP1-GFP and PROZIP1$^{CS\text{-}mut}$-GFP localize to the cytoplasm. In addition to maize protoplasts, PROZIP1-mcherry constructs were also expressed for co-localization with GFP in *N. benthamiana* leaves. Confocal microscopy 3 dpi after *A. tumefaciens* showed similar results as the maize protoplasts (Fig. S2B). Together, microscopic analysis suggests a cytoplasmic and nuclear localization of PROZIP1, which is independent from the mutation at the predicted cleavage sites in both maize and *N. benthamiana*. To determine whether endoplasmic reticulum (ER) localization could provide a possible explanation for the observed signals in the nuclear periphery, PROZIP1-GFP and PROZIP1$^{CS\text{-}mut}$-GFP were further analyzed by confocal microscopy using mCherry fused with KDEL, a known ER localization signal, as a control (Napier *et al*., 1992; Griffiths *et al*., 1994). PROZIP1-GFP and PROZIP1$^{CS\text{-}mut}$-GFP co-localized with mCherry-KDEL (Fig. 2B), supporting an ER-associated localization of PROZIP1. Based on these microscopic observations we hypothesized that PROZIP1 initially localizes to the ER, where its proteolytic processing is likely initiated.

N-terminal cleavage of PROZIP1 is required for its translocation

To monitor processing events of PROZIP1, *N. benthamiana* leaves expressing PROZIP1-GFP and PROZIP1$^{CS\text{-}mut}$-GFP were subjected to subcellular fractionation and Western blot analysis using either an α-GFP or α-Zip1 antibody. Antibodies for α-RuBisCO (cytosol), α-Histone H3 (nucleus), and α-Bip (microsome) were used as markers for subcellular compartments. Total protein extract (TE) served as input control containing full length PROZIP1-GFP at 43 kDa and processed fragments containing Zip1 at ca. 34 kDa, 35 kDa and 28 kDa (Fig. 3A, left panel). PROZIP1$^{CS\text{-}mut}$-GFP TE sample showed the full-length protein at 43 kDa together with processed Zip1-containing fragments at ca. 38 kDa and 28 kDa (Fig. 3A, right panel). Similar cleavage fragments of PROZIP1-GFP were observed in the cytosolic (34 kDa and 35 kDa) and microsomal (35 kDa) fractions, while no signals were detected in the nuclear fractions, supporting KDEL co-localization observed in confocal microscopy (Fig. 2C). A weaker signal for PROZIP1-GFP than for PROZIP1$^{CS\text{-}mut}$-GFP (ca. 43 kDa) was detected in the cytosolic fraction using α-Zip1 (Fig. 3A), suggesting stabilization of the full-length PROZIP1$^{CS\text{-}mut}$-GFP construct. Processed fragments of PROZIP1$^{CS\text{-}mut}$-GFP (37 kDa and 39 kDa) and PROZIP1-GFP (34 kDa and 36 kDa) were mainly observed in the cytosol and TE (Fig. 3A). Processing of PROZIP1$^{CS\text{-}mut}$-GFP was not observed in the microsomal fraction, suggesting that the mutations lead to an altered intracellular processing compared to native PROZIP1-GFP. Microsomal processing of PROZIP1 may explain the increased vesicle trafficking between the ER and plasma membrane observed by RNA-seq after Zip1 treatment (Fig. S1D). This is particularly significant given that Zip1 is an apoplastic peptide released from PROZIP1, which lacks a typical secretion signal (Ziemann et al., 2018; Del Corpo et al., 2024). In the apoplast, PROZIP1$^{CS\text{-}mut}$-GFP was predominantly detected as its full-length protein (43 kDa). In contrast, PROZIP1-GFP showed a Zip1-containing signal at 34 kDa, similar to the one observed in the cytosol, suggesting that this fragment is translocated from the cytosol to the apoplast (Fig. 3A). Together, these results suggest that PROZIP1 undergoes intracellular N-terminal processing prior to secretion.

To investigate the cleavage pattern of the N-terminal region of PROZIP1 (PROZIP1$^{1\text{-}70}$), which does not contain the Zip1 peptide (Fig. 3C), we constructed a N-terminal GFP fusion protein for PROZIP1$^{1\text{-}70}$-GFP and PROZIP1$^{1\text{-}70_CS_mut}$-GFP, which contains two RR-motifs mutated to AA (RR$^{25\text{-}26}$ to AA$^{25\text{-}26}$ and RR$^{50\text{-}51}$ to AA$^{50\text{-}51}$). TE of PROZIP1$^{1\text{-}70}$-GFP showed mainly two bands at ca. 37 kDa (full-length) and

20 kDa. The cytosolic fraction showed three bands at 36 kDa, 34 kDa and 20 kDa, whereas the microsomal fraction showed two faint bands at 36 kDa and 20 kDa (Fig. 3B, left panel). In contrast, PROZIP1$^{1\text{-}70_CS\text{-}mut}$-GFP showed unspecific cleavage resulting in a laddering pattern in both, the cytosolic and the microsomal fraction (Fig. 3B, right panel). The GFP control showed a main signal at 28 kDa (full-length) and a cleavage product at ca. 20 kDa, indicating that the signals at 20 kDa observed for PROZIP1$^{1\text{-}70}$-GFP and PROZIP1$^{1\text{-}70_CS\text{-}mut}$-GFP might derive from GFP cleavage products (Fig. 3A and Fig. 3B). Based on the observed cleavage patterns, we hypothesized that the two RR-motifs (RR$^{25\text{-}26}$ and RR$^{50\text{-}51}$) might serve as specific processing sites and that their mutations result in miss-cleavage or proteolytic degradation. These data suggest that processing of the N-terminal region of PROZIP1$^{1\text{-}70}$ might be important to release the C-terminal PROZIP1 (Ct-PROZIP1) into the cytosol, followed by a subsequently translocation into the apoplast.

To investigate if PROZIP1$^{1\text{-}70}$-GFP harbors characteristics of lipophilic domains, which could explain PROZIP1 microsome associated localization, a hydropathy plot was generated. PROZIP1 displays a decreasing hydrophobicity gradient from the N- to the C-terminus, with the N-terminal region showing the highest lipophilicity, suggesting a potential membrane association (Fig. 3C).

To confirm the release of Zip1 into the apoplast, subcellular fractions were subjected to an ELISA assay (Koenig *et al*., 2025). Zip1-containing fragments were detected in the microsome, cytosol and apoplast of PROZIP1-GFP and PROZIP1$^{CS\text{-}mut}$-GFP (Fig. 3D). Signal quantification suggests that Zip1-containing fragments are more abundant in the cytosolic and microsomal fractions of PROZIP1$^{CS\text{-}mut}$-GFP compared to PROZIP1-GFP (Fig. 3D), correlating with the abundance observed in Western blot analysis (Fig. 3A). Zip1-containing fragments were absent in the nuclear fraction of both PROZIP1-GFP and PROZIP1$^{CS\text{-}mut}$-GFP samples in agreement with the Western blot analysis, (Fig. 3D). Notably, significant numbers of Zip1-containing fragments were found in the apoplast of PROZIP1-GFP, indicating an impaired processing or release in the PROZIP1$^{CS\text{-}mut}$-GFP sample (Fig. 3D). To distinguish Zip1 from Zip1-containing fragments, the apoplastic fluids of PROZIP1-GFP and PROZIP1$^{CS\text{-}mut}$-GFP were size separated with a 5 kDa cut-off, and both high molecular weight fraction (HMW) and low molecular weight fraction (LMW) fractions were analyzed by ELISA. No significant differences of Zip1 abundance were detected in the HMW of PROZIP1-GFP and PROZIP1$^{CS\text{-}mut}$-GFP (Fig. 3E). In contrast, Zip1

was exclusively detected in the LMW fraction of apoplastic PROZIP1-GFP, indicating that Zip1 is released into the apoplast and that the release of Zip1 from PROZIP1$^{CS\text{-}mut}$-GFP is impaired.

Since microsome-related genes were significantly upregulated after Zip1 treatment (Fig. 1C and Fig. S1D), we tested whether Ct-PROZIP1 might be translocated into the apoplast via an unconventional secretion pathway. Therefore, PROZIP1-GFP was co-expressed with Sar1A or Sar1B in *N. benthamiana* leaves (Fig. 3F). Sar1A and Sar1B are essential regulators of COPII vesicle formation and ER-to-Golgi transport. Their overexpression disrupts ER homeostasis and inhibits conventional protein secretion (Barlowe *et al*., 1994; Memon *et al*., 2004; Cevher-Keskin *et al*., 2013). Additionally, leaves were pre-treated with brefeldin A (BFA), concanamycin A (ConA) and wortmannin (Wm) prior to PROZIP1-GFP expression. Similar to Sar1 overexpression, BFA blocks secretion at the ER–Golgi interface (Nebenfuhr *et al*., 2002), thereby blocking the conventional secretory pathway. ConA and Wm can indirectly impair unconventional secretion pathways: ConA blocks V-ATPases, preventing organelle acidification and thereby disrupting pH-dependent sorting, trafficking, and degradation in secretory and lytic pathways (Robinson *et al*., 2004). Wm inhibits PI3K and PI4K at high doses, disrupting phosphoinositide production and impairing endosomal trafficking, MVB formation, and autophagy (Takac *et al*., 2012). GFP fused to the signal peptide of *N. tobacco* PR1 (spNtPR1-GFP) served as a control for the conventional secretion pathway (Niderman *et al*., 1995). We found that BFA treatment, Sar1A and Sar1B overexpression do not affect the accumulation of Ct-PROZIP1-GFP in the apoplast, indicating trafficking of Ct-PROZIP1-GFP via the unconventional secretion pathway (Fig. 3F). ConA treatment significantly reduced the accumulation of Ct-PROZIP1-GFP in the apoplast, similarly to the Wm treatment (Fig. 3F). In contrast, spNtPR1-GFP release was significantly inhibited by BFA and Sar1 overexpression, but not by ConA, Wm or the combination. These results indicate that Ct-PROZIP1 requires unconventional secretion for translocation into the apoplast.

Intracellular arginine-dependent processing of PROZIP1

We next adapted amino-terminal oriented mass spectrometry of substrates (ATOMS) to identify *in-vivo* generated PROZIP1 cleavage products and to determine their cleavage sites and the peptides released during PROZIP1 processing

(Doucet *et al*., 2011). PROZIP-GFP and PROZIP1$^{CS\text{-}mut}$-GFP were over-expressed in maize protoplasts and in *N. benthamiana* leaves (Fig. 4A and Fig. S3). GFP-containing C-terminal fragments were enriched by GFP-immunoprecipitation and primary amines were labeled by reductive demethylation with $^{13}CDO_2$-formaldehyde to mark the N-terminal amines of PROZIP1 cleavage products. Mass spectrometric analysis identified mostly C-terminal cleavage products of both, PROZIP1-GFP and PROZIP1$^{CS\text{-}mut}$-GFP, likely due to the enrichment of GFP-containing fragments. In both, maize and *N. benthamiana*, the identified peptides were highly similar, indicating that the proteases responsible for PROZIP1 processing are conserved between these species (Fig. 4A, Fig. S3, Tables S2 and S3). The cleavage pattern suggests an arginine-dependent mechanism, as most peptides were released immediately before or after a double arginine (RR) motif. The peptide QPWEGESELKLATQGASVR$^{85\text{-}103}$ shares substantial overlap with the bioactive Zip1 peptide (EGESELKLATQGASVRR$^{88\text{-}104}$) (Ziemann *et al*., 2018). One identified PROZIP1 peptide, EIQAOSVEFR$^{71\text{-}80}$, located at the N-terminal of the Zip1-containing fragments, was extended in PROZIP1$^{CS\text{-}mut}$ (Fig. 4A). This suggests that mutations in the nearby N- and C-terminal RR-motifs (RR$^{69\text{-}70}$, (F)RR$^{79\text{-}81}$) affect the proteolytic cleavage of PROZIP1. A major cleavage fragment of PROZIP1-GFP (36 kDa), previously observed in the anti-Zip1 western blot (Fig. 3A), is likely generated by cleavage at the N-terminal RR-motifs (RR$^{25\text{-}26}$, RR$^{50\text{-}51}$, RR$^{69\text{-}70}$), producing a new N-terminus (E^{71}). PROZIP1-GFP, lacking this N-terminal fragment, has a predicted molecular weight of 34.6 kDa, which correlates to the major band observed in GFP- and Zip1-blots (Fig. 3A). Notably, no Zip1 peptide was identified in PROZIP1$^{CS\text{-}mut}$-GFP (Fig. 4A and Table S3). This suggests that RR-motif mutations prevent Zip1 release and strongly impaired Ct-translocation (Fig. 3D, Fig. 4A). Additionally, cleavage at two single arginine sites (R^{84}, R^{106}) was observed at the N- and C-termini of Zip1 within PROZIP1, suggesting that single arginine residues can contribute to Zip1 release (Fig. 4A).

3D structures of PROZIP1 and PROZIP1CS-mut were modeled using I-TASSER, yielding scores of -4.39 and -4.21, respectively, indicating high structural reliability. Eight putative cleavage sites were identified in PROZIP1, corresponding to surface-exposed arginine residues, indicating their potential accessibility to proteolytic enzymes (Fig. 4B). In contrast, in PROZIP1$^{CS\text{-}mut}$ the N-terminal arginine residues (RR$^{25\text{-}26}$, RR$^{50\text{-}51}$; light blue) were buried. Furthermore, Zip1 in PROZIP1 was

positioned outwards, creating a cavity between residues, which is absent in PROZIP1$^{CS\text{-}mut}$, that might facilitate enzyme binding for enzymatic cleavage.

A key structural difference was the N-terminal region (white fragment, Fig. 4B), which appeared bulky in PROZIP1, but not in PROZIP1$^{CS\text{-}mut}$. PROZIP1 formed a self-contained, chain-like structure, whereas PROZIP1$^{CS\text{-}mut}$ resembled a twisted, adhesive string. In conclusion, we identified eight cleavage sites in PROZIP1, all featuring arginine in P1 position. The 3D models support an arginine-dependent cleavage mechanism, as these arginine residues are surface-exposed and likely accessible to proteases.

Intracellular PROZIP1 is processed by maize metacaspase ZmMC9

Intracellular arginine-dependent cleavage highlights metacaspases (MCAs) as promising candidate proteases. MCAs typically cleave substrates at arginine residues and have been shown to process phytocytokines in *Arabidopsis thaliana*. For example, AtMC4 cleaves ProPep1 and AtMC9 cleaves ProGRI, the precursors of Pep1 and the Grim Reaper peptide, respectively (Stael *et al*., 2022; Wrzaczek *et al*., 2015). AtMC4 and AtMC9 are classified as type II MCAs, characterized by the presence of a p20 domain, followed by a linker sequence that connects the p20 domain to a subsequent p10 domain (Huh *et al*., 2022), and the absence of an N-terminal extension typical for type I MCAs (Fig. 5A). We observed cleavage of PROZIP1, but not of PROZIP1$^{CS\text{-}mut}$ *in vitro* using purified AtMC4 (Fig. S4 and Fig. S5). The finding that AtMC4 cleaves PROZIP1 prompted us to investigate endogenous maize MCAs. A phylogenetic analysis comprising maize and Arabidopsis MCAs revealed eight type I MCAs and three type II MCAs, of which the maize ZmMC9 (ZmMCA-IIa) and ZmMC10 (ZmMCA-IIb) are the closest homologues of the Arabidopsis calcium-dependent AtMC4, while ZmMC11 (ZmMCA-IIc) is more similar to the low pH-dependent AtMC9 (Fig. 5B).

As the p20 domain contains the active sites (H^{88}, C^{141}) (Zhu *et al*., 2020) and Ca^{2+}-binding sites (D^{101}, Q^{119}, D^{120}, D^{148}) (Huh *et al*., 2022), we compared the conservation of these p20 domain motifs of the three maize MCAs to AtMC4 and AtMC9 (Fig. 5C). While the active sites are conserved among all of the five MCAs, the Ca^{2+}-binding sites of AtMC9 and ZmMC11 were not. Also, the overall similarity of AtMC9 and ZmMC11 was lower compared to AtMC4 with ZmMC9 and ZmMC10, suggesting a possible divergence of ZmMC11 from ZmMC9 and ZmMC10.

Next, we analyzed RNA-seq data, focusing on the 6-hour time point due to its relevance for *Prozip1* expression and MCA activity. Four MCAs were found expressed: type II (ZmMC9, ZmMC10, ZmMC11) and type I (ZmMC5) (Fig. 5B, Fig. S6). While ZmMC10 and ZmMC11 were barely expressed, ZmMC9 and ZmMC5 showed moderate expression, but none were strongly induced by SA or Zip1. Notably, Zip1 significantly repressed ZmMC5, highlighting ZmMC9 as the primary candidate for PROZIP1 processing.

Both ZmMC9 and ZmMC10 were produced in *E. coli* and subsequently purified via affinity chromatography (Fig. S7A). The activity of recombinant AtMC4, ZmMC9 and ZmMC10 was monitored using the probe DK-13 via activity-based protein profiling (ABPP) (Strancar *et al*., 2022) (Fig. S7B, left and right panel). An active site mutant of ZmMC9 (ZmMC9_CA) was generated in which the catalytic residues cysteine and histidine were replaced by alanine, respectively. AtMC4_CA and ZmMC9_CA loss of activity was also tested via ABPP (Hander *et al*., 2019; Fig. 5D). Autocatalytic processing is impaired in the inactive mutants, resulting in a full-length inactive state (Fig. 5D, middle and bottom panel).

In-vitro cleavage assays were performed to determine the cleavage specificity of the maize MCAs (Fig. 5E and Fig. S7C-D). AtMC4 and ZmMC9, but not ZmMC10, cleaved PROZIP1, as indicated by the decrease of the PROZIP1 signal (Fig. S7C), suggesting distinct substrate specificities for ZmMC9 and ZmMC10. Furthermore, PROZIP1$^{CS\text{-}mut}$ remained more stable, confirming PROZIP1 arginine-dependent cleavage. However, cleavage of PROZIP1$^{CS\text{-}mut}$ by AtMC4 and ZmMC9 was observed, although it appeared less effective (Fig. S7D). To address the specificity of ZmMC9 and the observed cleavage of PROZIP1$^{CS\text{-}mut}$, ZmMC9 was tested in a concentration range (Fig. 5E). PROZIP1, as well as PROZIP1$^{CS\text{-}mut}$, were visibly processed by ZmMC9. 250nM ZmMC9 for 30 minutes were sufficient to significantly cleave PROZIP1 but not the PROZIP1$^{CS\text{-}mut}$.

The activity of ZmMC9 was found to directly depend on the presence of Ca^{2+} (Fig. 5F). Testing various protease inhibitors revealed that ZmMC9 activity is insensitive to E-64 (Fig. S7E), but sensitive to leupeptin in a concentration-dependent manner (Fig. 5G, left panel). Furthermore, a minimal concentration of 0.5 mM EDTA significantly reduced ZmMC9 activity (Fig. 5G, right panel), supporting the Ca^{2+}-dependency of ZmMC9. To obtain detailed insights into the cleavage site preference, we characterized ZmMC9 by proteomic identification of protease

cleavage sites (PICS) (Demir *et al*., 2022). This identified up to 1753 cleaved peptides that revealed a striking, strong preference for arginine at the P1 position of the ZmMC9 cleavage site (Fig. 5H), which perfectly matches the observed arginine-dependent cleavage of PROZIP1. Besides, a preference for a hydrophobic residue (valine, isoleucine, leucine) in P2 position was observed, which fits a hydrophobic S2´pocket that was previously described in the protein structures of AtMC4 and AtMC9 (Zhu *et al*., 2020; Stael *et al*., 2023).

PLCPs cleave C-terminal PROZIP1 in the apoplast

In previous work we proposed that PLCPs are responsible for the release of apoplastic Zip1 (Ziemann *et al*., 2018). Given that PROZIP1-GFP undergoes intracellular processing, we sought to test if PLCPs are involved in intracellular PROZIP1 processing and translocation. Maize protoplasts expressing PROZIP1-GFP or PROZIP1$^{CS\text{-}mut}$-GFP were treated with the cell-permeable, covalent PLCP inhibitor E64d, respectively (Fig. 6A-B). However, the subcellular localization of PROZIP1-GFP and PROZIP1$^{CS\text{-}mut}$-GFP was not affected by E-64d, suggesting that the activity of intracellular PLCPs might not be involved in their subcellular localization (Fig. 6A). Immunoblot analysis showed that the cleavage patterns of PROZIP1-GFP and PROZIP1$^{CS\text{-}mut}$-GFP were not affected by E-64d treatment. In contrast, ABPP of PLCPs using DCG04 labeling (Greenbaum *et al*., 2000) demonstrated effective inhibition of intracellular PLCPs (Fig. 6B). These findings indicate that intracellular cleavage of PROZIP1 occurs independently of PLCP activity. The predominant PROZIP1-GFP cleavage product (35 kDa) contains Zip1, as it is detected by the specific α-Zip1 antibody (Fig. 6B). In contrast, PROZIP1$^{CS\text{-}mut}$-GFP was primarily detectable in its full-length version (43 kDa), reflecting its failed processing as described above (Fig. 3A). Also, for PROZIP1$^{CS\text{-}mut}$-GFP three cleavage fragments at 17, 38, and 40 kDa were observed, which are likely attributed to the mutated double arginine motifs (Fig. 4A). Together, these results could not substantiate a role of PLCPs for intracellular PROZIP1 processing.

Next, we investigated PROZIP1 processing in the apoplast. Incubation with apoplastic fluid from SA-treated maize revealed a time-dependent cleavage of PROZIP1 (Fig. 6C, left panel). To assess the involvement of PLCPs, we applied the inhibitor E-64. In addition, pepstatin A (pepA), an inhibitor of aspartic proteases was used. Each inhibitor individually reduced PROZIP1 cleavage, indicating contributions

from both protease classes (Fig. 6C, middle panel). Combined application of E64 and pepA abolished PROZIP1 cleavage (Fig. 6C, right panel).

To identify peptides generated during extracellular cleavage PROZIP1 was co-incubated with a maize apoplastic fluid fraction enriched in active PLCPs, of which CP1 and CP2 were the most abundant (Misas Villamil *et al*. 2019). The PLCP enriched-fraction was tested in the presence (+) or absence (-) of E-64 together with an inhibitor mix (i-mix) containing PepA (aspartic proteases), DCI (serine protease inhibitor) and EDTA (metalloprotease inhibitor). Subsequent ATOMS analysis identified peptides exclusively derived from the C-terminal region of PROZIP1 (Fig. 6D), which is in agreement with the above-described observation that only Ct-PROZIP1 is secreted into the apoplast (Fig. 3). In the absence of E-64, PLCP activity led to two cleavage events at the P2 positions valine and phenylalanine (FRR□□–□^{1} and VRR^{1}□^{2}–^{1}□□), which are characteristic of PLCPs. Notably, these sites contain the arginine residues previously identified as PROZIP1 cleavage sites (Fig. 4B), suggesting that PLCPs may release Zip1 from Ct-PROZIP1 in the apoplast. Moreover, PLCP cleavage was also observed within the Zip1 peptide itself (K^{94}), implying that PLCPs and also other apoplastic proteases may contribute to signal clearance. Cleavage at $RR^{103\text{-}104}$ and D^{122} persisted in the presence of E-64, suggesting that this site may be targeted by proteases other than PLCPs.

Collectively, these findings demonstrate that the C-terminal PROZIP1 is proteolytically processed in the apoplast by PLCPs. While PLCPs are not required for the intracellular processing and release of PROZIP1/Zip1, they appear to target apoplastic Ct-PROZIP1 to timely release Zip1 and also contribute to signal inactivation or clearance.

Discussion

In this study, we disclosed a two-step mechanism for processing and release of the maize phytocytokine Zip1. We demonstrated that primary processing of PROZIP1 occurs inside the cell and it is required as maturation step prior to Zip1 release and clearance. Cleavage of PROZIP1 occurs at specific arginine residues and is intracellularly catalyzed by the maize metacaspase ZmMC9. In a second step, the processed C-terminal PROZIP1 exits the cell via an unconventional protein secretion pathway and is cleaved by PLCPs to release Zip1 followed by its degradation for signal clearance (Fig.7).

SA and Zip1 are inducers of *Prozip1* expression, confirming a previously proposed positive feedback loop in which Zip1 amplifies SA-associated defense (Ziemann *et al*., 2018). Phytocytokine signaling is a highly dynamic process, where timing after the elicited signaling is crucial. While late Zip1 signaling responses at 24 hpi largely overlapped with SA signaling (Ziemann *et al*., 2018), the transcriptomic responses to both stimuli strongly diverged at early time points from 3-9 hpi. At this stage Zip1-induced gene regulation merely reflects intracellular processing and translocation, contrasting the general immune activation that is triggered by SA.

PROZIP1 undergoes primary processing steps, resulting in further cleavage within the cytosol (Fig. 7D-F), generating a pre-mature Ct-PROZIP1 that is subsequently observed in the apoplast (Fig. 7G). This processing likely reflects a regulatory step of phytocytokine maturation, in which PROZIP1 is kept in a steady-state awaiting activation and processing by the protease. The identification of eight cleavage sites after arginine residues in PROZIP1 led us to the assumption that metacaspases might be involved in its processing. Metacaspases cleave their substrates at the P1 position to basic amino acid residues, specifically arginine (R) and lysine (K), typically within a dibasic (R/K)x(R/K) cleavage motif (Vercammen *et al*., 2004). Although deviations from the canonical cleavage motif are observed, for instance in AtMC9 substrates (Tsiatsiani *et al*., 2013; Wrzaczek *et al*., 2015). Similarly, Arabidopsis PROPEP1 also lacks a double-basic motif (Hander *et al*., 2019). ZmMC9 is the only type II metacaspase that is co-regulated with *prozip1* expression and it has been shown to play a role in defense responses (Ahmad *et al*., 2012; Luan *et al*., 2021; Ma *et al*., 2021). It is localized to the cytosol (Luan *et al*., 2021; Ma *et al*., 2021) where its activation requires an increase in cytosolic Ca^{2+}, a phenomenon observed in response to cellular damage or pathogen attack (Fig. 7D) (Hander *et al*., 2019; Stael *et al*., 2022; Garcia *et al*., 2022). In damaged Arabidopsis cells, increased cytosolic Ca^{2+} activates AtMC4, leading to the release of the phytocytokine Pep1. In the absence of damage, this process is suppressed and the Pep1 precursor PROPEP1 is sequestered at the vacuolar membrane (Hander *et al*., 2019).

Zip1 treatment induced genes associated with Ca^{2+}-mediated processes including Ca^{2+} sensors, receptors, kinases, and proteins implicated in Ca^{2+} transport. Zip1 perception might therefore elicit the activation of ZmMC9, which cleaves PROZIP1 internally at the N-terminus, initiating the release of C-terminal PROZIP1 into the apoplast. Furthermore, the arginine-specificity exhibited by ZmMC9 aligns with the

identified cleavage sites and processing events, thereby substantiating ZmMC9 role in PROZIP1 processing. In future work, maize ZmMC9 knockout mutants may offer a means to confirm the internal cleavage required for further translocation of Ct-PROZIP1 to the apoplast.

Intracellular processing of propeptides has been reported for other phytocytokine precursors, including PROPEPs, GRIp, and PRORALF23 (Hander *et al*., 2019, Wrzaczek *et al*., 2015, Srivastava *et al*., 2009). These precursors are intracellularly processed to enable the translocation and ultimately apoplastic release of the bioactive phytocytokines. Other precursors of signaling peptides such as PR1, the precursor of CAPE9, undergoes processing in the apoplast and does not require intracellular maturation (Chen *et al*., 2023). In addition, there are phytocytokines such as PSK1 and PSY1 where the translocation requires a posttranslational modification (sulfonation), and the peptide release occurs in the apoplast by subtilase-mediated processing (Sauter *et al*., 2015, Tost *et al*., 2021, Shen *et al*., 2023). How phytocytokines leaves the cell to fulfill their function is still insufficiently understood. One proposed mechanism is the secretory pathway. Phytocytokine precursors that undergo conventional secretion include Pre-PROPSK1/4, Pre-PRORGF7/GLV4, Pre-PRORGF9/GLV2, Pre-PROPSY1, Pre-PROSCOOP12, Pre-PRORALF23, while others such as PROSYS and PROPEP1 are hypothesized to release active phytocytokines via unconventional secretion or damage-induced cell bursting (Hou *et al*., 2021; Del Corpo *et al*., 2024). Like PROPEP1, PROZIP1 does not possess a conventional secretion signal and therefore must undergo unconventional secretion. The transcriptional induction of genes involved in vesicular trafficking, secretion and endocytosis by Zip1 suggests exocytosis as a possible route for the translocation of Ct-PROZIP1 into the apoplast. This is in accordance with the finding that chemical inhibitors of the secretory pathway such as brefeldin A did not significantly reduce the accumulation of Ct-PROZIP1 in the apoplast. An alternative mechanism of secretion is mediated by EXPO (exocyst-positive organelles) (Wang *et al*., 2010). EXPO are double-membrane vesicles distinct from Golgi, TGN, MVB, and autophagosomes, not marked by typical endomembrane markers nor affected by the brefeldin A treatment. EXPO-mediated release of phytocytokines without conventional secretion signals has been recently hypothesized (Del Corpo *et al.,* 2024) and in humans, cytokines such as interleukin-beta are released similarly via ER-Golgi independent pathways (Galozzi *et al*., 2021). Secretion of immunogenic peptides via nonconventional routes

might also be driven by an evolutionary arms race with microbial pathogens. This is exemplified by the rice blast effector Avr-Pii which interacts with the Exo70 interface to interfere with exocytosis, thereby compromising host immune responses (de la Concepción *et al*., 2022).

After translocation into the apoplast Ct-PROZIP1 must be maturated to release the Zip1 peptide that was found in the apoplast (Ziemann *et al*., 2018). The apoplastic maize immune proteases CP1 and CP2, which are the most abundant apoplastic PLCPs activated upon SA signaling (van der Linde *et al*., 2012a) were proposed to cleave PROZIP1 in the apoplast releasing the bioactive Zip1 (Ziemann *et al*. 2018). We now found that PLCPs are not involved in the intracellular processing of PROZIP1, but cleave the secreted C-terminal in the apoplast (Fig. 7H). Cleavage outside of Zip1 results in its release whereas inside likely generates an inactive phytocytokine. This suggests that PLCPs contribute to Zip1 release and signal clearance in the apoplast, likely in concert with other apoplastic proteases (Fig. 7K). Such kind of mechanism was recently reported for the flg22 peptide, a major bacterial MAMP, which is released, but also degraded by the Arabidopsis subtilase SBT5.2 (Buscaill *et al*., 2024). In the case of flg22, SBT5.2 might modulate flagellin-triggered immunity by providing spatial and temporal regulation, thereby limiting excessive immune activation. Based on our findings, we propose a similar mechanism by which PLCPs provide a spatial and temporal regulation of Zip1 to modulate extracellular phytocytokine signaling. In this model, apoplastic release and degradation of bioactive Zip1 is controlled by PLCPs to ensure transient amplification, but also restriction of immune signaling.

Together, our findings uncover a two-step mechanism governing PROZIP1 phytocytokine maturation: an initial intracellular cleavage driven by the ZmMC9 metacaspase, followed by an apoplastic activation and clearance phase where PLCPs regulate the spatial and temporal degradation of Zip1. This highlights a tightly controlled regulatory mechanism that coordinates critical steps in plant immune signaling.

Material and Methods

Plant growth conditions

Grains of maize (*Z. mays*, cv. Golden Bantam, B73 and Ky21) were placed in organic growth soil and were grown for 7 to 8 days in a plant growth chamber (15 h light at

28 °C, ~1000 µmol m^{-2} s^{-1}; 1 h twilight; 7 h dark at 22 °C). *N. benthamiana* plants were grown for six weeks in the university's greenhouse at 23°C on a long day period (16 h light) and at 20°C for 8h in the dark with 30% to 40% humidity.

Plant treatments

Zip1 (QPWEGESELKLATQGASVR), lyophilized peptide powder was diluted to stock concentrations of 0.5 mg/ml. The final concentration to treat the plants was 4 µM. Salicylic acid (SA) powder was dissolved in 1% DMSO and added to water at a final concentration of 2mM SA. The second leaf of 8-day-old maize seedlings was infiltrated, using a 1-ml needleless syringe.

Gene expression analyses and RNAseq

Leaf samples were collected 6 hours post-inoculation (hpi) and ground in liquid nitrogen. Total RNA was extracted using the TRIzol reagent (Ambion Life Technologies) according to the manufacturer's protocol. To eliminate genomic DNA contamination, the RNA was treated with TURBO DNA-free reagents following the corresponding guidelines. 3µg of total RNA were reverse transcribed into complementary DNA (cDNA) using the RevertAid H Minus First Strand cDNA Synthesis Kit (Thermo Scientific), employing the oligo(dT)$_{18}$ primer and *Prozip1* specific primer. The resulting cDNA was diluted 1:100 with nuclease-free water and subsequently used for qRT-PCR with gene-specific primers. Detection was performed using the iQ SYBR Green reagent (Promega). GAPDH served as the reference gene. The gene *Wrky65*, were included as marker for SA signaling pathways. RNA samples of Zip1, SA and mock (water) were sent for RNA sequencing (Novogene). RNA libraries were prepared using an Illumina TruSeq paired-end sequencing (Illumina, SanDiego, CA, USA) performed on a HiSeq4000 platform. Reads of three biological replicates were filtered using the Trimmomatic software 0.39 and standard settings and mapped to a reference assembly using BOWTIE2 (version 2.3.4.1) (Langmead & Salzberg, 2012). Zm-B73-Reference-NAM-5.0 was used as the reference genome and was obtained from maizegdb.org. Reads were counted using HTse1-count (version 2.0.4) (Anders *et al*., 2015).

Microscopy and E-64 treatments of maize protoplasts

Maize protoplasts were generated according to Koenig *et al*. (2025) and transfected with PROZIP1-GFP, PROZIP1$^{CS\text{-}mut}$-GFP, NLS-mCherry or mCherry-KDEL. For E64 treatments protoplasts were treated with 30 µM E-64 or E-64d after the transfection. After 16h, protoplasts were subjected to microscopy. A set of the samples were used for Western Blot analysis. Protein was extracted in 50mM NaOAc buffer pH 6 and labeled for 1h with 1µM DCG04-biotin probe. Samples were detected by Weszern blot usiung Zip1-, GFP- and Streptavidin antibody.

Agrobacterium-mediated transformation of _N. benthamiana_

Required strains of *Agrobacterium tumefaciens* strains were resuspended in 10 mM MgCl2 to an OD600 of 1.0. Test strains were mixed 1:1 (v/v) with P19 strain and a final concentration of 200µM acetosyringone was added to the cultures. The bacterial suspensions were infiltrated on the abaxial side of the leaves using needless 1 mL disposable syringes. Leaf material was collected after 2 or 3 days, respectively.

Subcellular compartment separation

Transformed *N. benthamiana* plants (3 dpi) were used for the analysis. Full extract (FE), apoplastic fluid (AF), a nuclear fraction (nucleus), a microsome fraction (Micro) and the cytosol were generated. FE: SDS sample buffer was added to ground leaf powder. AF: Fresh leaves were vacuum infiltrated at 240 mbar for 3x10 minutes. The leaves were placed vertically into 20 ml needleless syringes and the syringes were placed in 50 mL falcon tubes. Tubes were centrifuged at 2000 g for 15 minutes at 4°C. AF was separated in a high molecular weight fraction (> 5 kDa) and a low molecular weight fraction (> 5 kDa) using Spin columns (Amicon Ultra, REF: UFC800324. 1 mL AF was loaded onto the columns and centrifuged at 4000g for 60 min. 25 µL of flow through was diluted 1:1 (v/v) using ELISA coating buffer and then subjected to ELISA for coating. The membrane of the column was flushed with coating buffer (same volume then the used AF) and liquid was transferred to a sample tube. 50µL of the liquid were used for the coating (ELISA-assay) as the high molecular weight fraction. Nuclear fraction: 1.5 g of full extract was used, and we followed the procedure published by Xu and Copeland (2012). For cytosol and microsome we used the protocol from Zhao and Li (2017).

BFA A, ConA and Wm treatment and Sar1 overexpression

N. benthamiana plants were treated with brefeldin A (10 µg/ml), ConA (0.5 µM) and Wm (35 µM) by leaf infiltration and left incubating for 4 hours. Next, PROZIP1-GFP was expressed by *Agrobacterium*-mediated transformation. Bacterial cultures expressing PROZIP1-GFP were mixed in a 1:1 ratio with P19 and Sar1 strains or P19 only, respectively. Apoplastic fluid was isolated 2 days post infiltration.

GFP pull-down for cleavage site mapping

Infiltrated leaves of *N. benthamiana* (3 dpi) were ground and the obtained leaf powder was used for the GFP pull-down using GFP-Trap Agarose beads (Chromotek Ref. gta). For maize protoplasts, 3 mL of $2*10^5$ transfected cells were used for GFP-Trap Agarose. The pull-downs were performed according to the manufacturers protocol. 10% of the obtained eluate were tested by Western blot and subsequently analyzed by mass spectrometry.

Expression and purification of recombinant PROZIP1 and PROZIP1$^{CS\text{-}mut}$

The DNA sequence of PROZIP1 was amplified and cloned into the pOPINM expression vector (His-MBP) using the In-Fusion Dry-Down PCR Kit (TARAKA). *E. coli* Shuffle was used for the expression of His-MBP-PROZIP1. Protein was purified by Ni-NTA (AC) and size exclusion chromatography (SEC). PROZIP1$^{CS\text{-}mut}$ was generated following the protocol of Ziemann *et al*. (2018).

Expression and purification of recombinant ZmMC9, ZmMC9_CA and ZmMC10

The sequence of ZmMC9 (Zm00001eb150730) and ZmMC10 (Zm00001eb352560) were obtained from maizegdb.org. 6h Zip1-treated cDNA samples, which were used for the RNAseq, were used for the amplification of both. Amplicons were cloned into the #3128 backbone harboring a T7 promoter, C-terminal His-Tag and T7 terminator. E. coli BL21 strains #3745 (ZmMC9) and #3746 (ZmMC10) were used for the expression.

Activity-based protein profiling of metacaspases

Activity-based protein profiling of metacaspases was performed as described before (Strancar *et al*., 2022). In short, a reaction mixture was set containing labelling buffer (20 mM HEPES, 150 mM NaC, 5 mM DTT), recombinant protease (5mg/ml), DK13 probe (0.5 µM) and $CaCl_2$ (5 mM). Labeling was performed for 1h at room temperature. To stop the reaction acetone was added (1:1 v/v) and pellet was

resuspended in PBS supplemented with 1% SDS. Next, click chemistry was performed by making a premix containing CuSO4 (1 mM), TCEP (2 mM) and TBTA (0.1 mM). Cy5 (2.5 mM) was added followed by 3.5 µL of premix (1h at room temperature). Protein was precipitated and Laemmli buffer was added. Activity was visualized after the samples run on SDS PAGE by fluorescence (Cy5 filter) scanning.

Metacaspase *in vitro* cleavage assays

4x Reaction buffer (200 mM HEPES pH 7.5, 600 mM NaCl, 40% glycerol, 200 mM CaCl2) supplemented with DTT (40 mM) was mixed with water and substrate. Next, metacaspase in protease dilution buffer (25 mM HEPES pH 7.5, 50% glycerol) was added. Reactions were incubated (30 min at room temperature) and were stopped by Laemmli buffer (SDS PAGE) or ELISA coating buffer supplemented with EDTA and leupeptin. ELISA samples were frozen immediately. ELISA samples were diluted 1:10 with coating buffer and inhibitors prior coating.

Proteomic Identification of protease Cleavage sites (PICS)

ZmMC9 cleavage site specificity was tested with *E. coli* proteome-derived peptide libraries as described (Demir et al 2022). 22.5 µM of purified ZmMC9 and the active site mutant ZmMC9_CA were incubated with 40µg of legumain-digested peptide library and incubated for 1h and 16h. Reactions were stopped by a mix of 100 µM leupeptin and 10 mM EDTA and samples were frozen at -80°C before acidification with 0.5% TFA and desalting using in-house packed C18 STAGE tips (Rappsilber et al 2007). Next, the analysis was conducted with an Orbitrap Elite mass spectrometer (Thermo) coupled to an UltiMate 3000 RSLCnano HPLC system (Thermo) operated in a two-column setup (nanoEase™ M/Z Symmetry C18 precolumns, 20 mm x 180 µm inner diameter, and nanoEase™ M/Z HSS C18 T3 analytical column, 250mm x 75 µm inner diameter; Waters). Peptides were eluted at a flow rate of 0.3 µl/min and column oven temperature of 40°C using a binary gradient (solvent A 0.1% (v/v) formic acid (FA); solvent B 0.1% (v/v) FA, 50% (v/v) methanol (MeOH), and 30% (v/v) acetonitrile (ACN)). This system was interfaced online with the Nanospray Flex ion source featuring the PST-HV-NFU liquid junction (MS Wil) and fused silica emitters (EM-20-360; MicrOmics Technologies LLC). The following parameters were applied for MS1 scans: mass range of m/z 370 - 1,700, a resolution of 120,000 (at m/z 400), a target value (AGC) of 1 x 10^6 ions, and a maximum injection time (IT) of 200 ms.

For MS2 scans, up to 15 most intense precursor peptides with a charge ≥ 2 were selected for collision induced dissociation (CID) in the linear trap with a normalized collision energy of 35%, activation time 10 sec q-value = 0.25, an AGC of 5000 ions, a max. IT of 150 ms, and dynamic exclusion for 45 s. Database searches were performed using the software MaxQuant (version 2.4.2.0), with settings as described (Demir et al. 2022) and differentially cleaved peptides were identified with the PINCIS script (v.12) as described (Demir et al 2022). Cleavage site preference was visualized using the iceLogo webserver (Maddelein *et al*., 2015).

PROZIP1 cleavage site mapping

For mapping of cleavage sites in PROZIP1-GPF in vivo, immunoprecipitated samples were differential dimethyl labeled with 40 mM sodium cyanoborohydride and 40 mM light formaldehyde ($^{12}CH_2O$; for PROZIP1-GFP samples) or heavy formaldehyde ($^{13}CD_2O$, for PROZIP1^{CS}-GFP samples), followed by digestion with trypsin or legumain as described (Soh *et al*., 2020). For PROZIP1 processing by PLCP-containing apoplast fractions, 45 µl of each PROZIP1 sample was treated with an apoplast fluid fraction enriched in PLCPs (Misas Vilamil *et al*., 2019) in the presence of an inhibitor mix with or without E-64, denatured and differential dimethyl labeled with 40 mM sodium cyanoborohydride and 40 mM formaldehyde ($^{12}CH_2O$ for PROZIP1 incubated in the presence of E-64, $^{13}CD_2O$ for samples without E-64). All peptide samples were acidified with 2 % of formic acid (pH 2.5) and desalted using in-house packed C18 STAGE tips (Rappsilber et al 2007). Eluted peptides were dried in a vacuum concentrator, resolved in 10 µl 2 % (v/v) acetonitrile, 0.05 % (v/v) TFA and separated on a HPLC system operated in a two-column setup (for in vitro dataset: 2 cm Acclaim PepMap RP trap and 15 cm Acclaim PepMap 100 column Acclaim PepMap, Thermo; for in vivo datasets: 2 cm PAC trap column, 50 cm PAC analytical column, PharmaFluidics) using a binary gradient from 2% to 80% acetonitrile. The eluted peptides were ionized with a CaptiveSpray ion source (Bruker) and precursor and fragment ion spectra (of the Top14 precursor ions) acquired using a QqTOF tandem mass spectrometer (Impact II, Bruker) with a m/z range of 150 – 3000 on MS1 at 2 Hz. The 14 most abundant precursor ions were selected for collision induced dissociation (CID), with 45 s dynamic exclusion, and fragment ion spectra were recorded in a m/z range of 150 – 3000 with no preferred charge states. Data were analyzed with the MaxQuant software package (Tyanova et

al 2016) (v1.6.0.16 for in vitro dataset, v2.0.1.0 for in vivo datasets) using the Uniprot database *Zea mays* or an improved *N. benthamiana* (Kourelis *et al*., 2019) proteome databases with appended recombinant PROZIP1 (in vitro dataset) processing in vitro) or appended PROZIP1-GFP and PROZIP1^{CS-}GFP sequences. Common contaminant protein lists provided with the MaxQuant release were appended as well. Digestion mode was set to unspecific (for the *in vitro*) or semispecific (for *in vivo* datasets) and the appropriate dimethyl modifications considered as fixed Lys and variable N-terminal modification. Methionine oxidation and N-terminal acetylation were considered as additional variable modifications.

Data availability

Source data are provided in this paper. All data supporting the findings of this study that are not directly available within the paper (and its supplementary data) will be upon reasonable request available from the corresponding authors (GD, JCMV). Raw data of RNA-seq analysis are publicly accessible in the NCBI Gene Expression Omnibus (accession number: GSE299461). Mass Spectrometry data are publicly accessible in the PRIDE database (accession numbers: PXD064693 and PXD064635).

Acknowledgements

We thank Barbara Mauchbach and Sofia Dubusc for assisting with PROZIP1 construct cloning and confocal microscopy. Lukas Meschig is acknowledged for supporting cloning of ZmMC9 and ZmMC10. We are grateful to Ute Meyer for expert technical support. We thank Tolga Bozkurt and Enoch Yuen for providing Sar1A and Sar1B constructs, and to Marina Klemenčič, Katharina P. van Midden, and Renier van der Hoorn for providing the DK13 metacaspase probe and their valuable support. We gratefully acknowledge Carmen Castell and Frank Van Breusegem for their valuable support in the MCA-related work. This work was supported by the Deutsche Forschungsgemeinschaft (DFG) under project DO 1421/5-2, SFB1403 (project no. 414786233), and the Cluster of Excellence on Plant Sciences (CEPLAS, EXC 2048/1—project ID: 390686111).

Author Contributions

MK, GD, and JCMV designed the study. MK, GD and JCMV designed the experiments, PFH design the mass spectrometry experiments. MK conducted the experiments, ZS performed subcellular compartments. JCMV generated the PLCP fraction and conducted apoplastic PROZIP1 cleavage assays. MM, AP and PFH analyzed mass spectrometry data. SS and CC provided recombinant AtMC4 and helped MK to establish MC cleavage assays. MK wrote the manuscript with contributions from all authors.

Competing interests

The author(s) declare no conflict of interest.

Supplementary information

Figure S1. Zip1 treatment induces Prozip1 and modulates immunity

Figure S2. PROZIP1 is localized intracellularly

Figure S3. Arginine-dependent processing of PROZIP1 in *N. benthamiana*

Figure S4. Expression and purification of recombinant PROZIP1 and PROZIP1$^{CS\text{-}mut}$

Figure S5. PROZIP1, but not Zip1 is cleaved by AtMC4 *in-vitro*

Figure S6. Expression of metacaspases identified by RNA-seq

Figure S7. Purified maize metacaspases and their activity

Table S1. RNA-seq data

Table S2. Mass Spectrometry of *N. benthamiana* expressing mcherry-PROZIP1-GFP

Table S3. Mass Spectrometry of *Z. mays* protoplasts expressing PROZIP1-GFP

Table S4. Mass Spectrometry of recombinant PROZIP1 + PLCP-enriched fraction

References

Ahmad, R., Zuily-Fodil, Y., Passaquet, C., Bethenod, O., Roche, R., & Repellin, A. (2012). Ozone and aging up-regulate type II metacaspase gene expression and global metacaspase activity in the leaves of field-grown maize (Zea mays L.) plants. *Chemosphere, 87*(7), 789–795.

Anders, S., Pyl, P. T., & Huber, W. (2015). HTSeq—A Python framework to work with high-throughput sequencing data. *Bioinformatics, 31*(2), 166–169. https://doi.org/10.1093/bioinformatics/btu638

Barlowe, C., Orci, L., Yeung, T., Hosobuchi, M., Hamamoto, S., Salama, N., ... & Schekman, R. (1994). COPII: A membrane coat formed by Sec proteins that drive vesicle budding from the endoplasmic reticulum. *Cell, 77*(6), 895–907. https://doi.org/10.1016/0092-8674(94)90138-4

Bartels, S., Lori, M., Mbengue, M., Van Verk, M., Klauser, D., Hander, T., ... & Boller, T. (2013). The family of Peps and their precursors in Arabidopsis: Differential expression and localization but similar induction of pattern-triggered immune responses. *Journal of Experimental Botany, 64*(17), 5309–5321. https://doi.org/10.1093/jxb/ert330

Bedinger, P. A., Pearce, G., & Covey, P. A. (2010). RALFs: Peptide regulators of plant growth. *Plant Signaling & Behavior, 5*(11), 1342–1346. https://doi.org/10.4161/psb.5.11.12954

Beloshistov, R. E., Dreizler, K., Galiullina, R. A., Tuzhikov, A. I., Serebryakova, M. V., Reichardt, S., ... & Vartapetian, A. B. (2018). Phytaspase-mediated precursor processing and maturation of the wound hormone systemin. *New Phytologist, 218*(3), 1167–1178. https://doi.org/10.1111/nph.14568

Buscaill, P., Sanguankiattichai, N., Kaschani, F., Huang, J., Mooney, B. C., Li, Y., ... & van der Hoorn, R. A. (2024). Subtilase SBT5.2 inactivates flagellin immunogenicity in the plant apoplast. *Nature Communications, 15*(1), 10431. https://doi.org/10.1038/s41467-024-54790-1

Cevher-Keskin, B. (2013). ARF1 and SAR1 GTPases in endomembrane trafficking in plants. *International Journal of Molecular Sciences, 14*(9), 18181–18199. https://doi.org/10.3390/ijms140918181

Chen, Y. L., Lin, F. W., Cheng, K. T., Chang, C. H., Hung, S. C., Efferth, T., & Chen, Y. R. (2023). XCP1 cleaves pathogenesis-related protein 1 into CAPE9 for systemic immunity in Arabidopsis. *Nature Communications, 14*(1), 4697. https://doi.org/10.1038/s41467-023-40406-7

De la Concepcion, J. C., Fujisaki, K., Bentham, A. R., Cruz Mireles, N., Sanchez de Medina Hernandez, V., Shimizu, M., ... & Banfield, M. J. (2022). A blast fungus zinc-finger fold effector binds to a hydrophobic pocket in host Exo70 proteins to modulate immune recognition in rice. *Proceedings of the National Academy of Sciences, 119*(43), e2210559119. https://doi.org/10.1073/pnas.2210559119

Del Corpo, D., Coculo, D., Greco, M., De Lorenzo, G., & Lionetti, V. (2024). Pull the fuzes: Processing protein precursors to generate apoplastic danger signals for triggering plant immunity. *Plant Communications.* https://doi.org/10.1016/j.xplc.2024.100931

Demir, F., Kuppusamy, M., Perrar, A., & Huesgen, P. F. (2022). Profiling sequence specificity of proteolytic activities using proteome-derived peptide libraries. *Methods in Molecular Biology, 2447*, 159–174. https://doi.org/10.1007/978-1-0716-2079-3_13

Doucet, A., Overall, C. M., & Smith, J. C. (2011). Broad coverage identification of multiple proteolytic cleavage site sequences in complex high molecular weight proteins using quantitative proteomics as a complement to Edman sequencing. *Molecular & Cellular Proteomics, 10*(5), M110.003533. https://doi.org/10.1074/mcp.M110.003533

Felix, G., & Boller, T. (1995). Systemin induces rapid ion fluxes and ethylene biosynthesis in Lycopersicon peruvianum cells. *The Plant Journal*, 7(3), 381–389. https://doi.org/10.1046/j.1365-313X.1995.7030381.x

Galozzi, P., Bindoli, S., Doria, A., & Sfriso, P. (2021). The revisited role of interleukin-1 alpha and beta in autoimmune and inflammatory disorders and in comorbidities. *Autoimmunity Reviews, 20*(4), 102785. https://doi.org/10.1016/j.autrev.2021.102785

Garcia, N., Kalicharan, R. E., Kinch, L., & Fernandez, J. (2022). Regulating death and disease: Exploring the roles of metacaspases in plants and fungi. *International Journal of Molecular Sciences, 24*(1), 312. https://doi.org/10.3390/ijms24010312

Ghorbani, S., Hoogewijs, K., Pečenková, T., Fernandez, A., Inzé, A., Eeckhout, D., Kawa, D., De Jaeger, G., Beeckman, T., Madder, A., Van Breusegem, F., & Hilson, P. (2016). The SBT6.1 subtilase processes the GOLVEN1 peptide controlling cell elongation. *Journal of Experimental Botany, 67*(16), 4877–4887. https://doi.org/10.1093/jxb/erw241

Greenbaum, D., Medzihradszky, K.□F., Burlingame, A., & Bogyo, M. (2000, August). Epoxide electrophiles as activity-dependent cysteine protease profiling and discovery tools. *Chemistry & Biology, 7*(8), 569–581. https://doi.org/10.1016/S1074-5521(00)00014-4

Griffiths, G., Ericsson, M., Krijnse-Locker, J., Nilsson, T., Goud, B., Söling, H. D., ... & Hong, W. (1994). Localization of the Lys, Asp, Glu, Leu tetrapeptide receptor to the Golgi complex and the intermediate compartment in mammalian cells. *Journal of Cell Biology, 127*(6), 1557–1574. https://doi.org/10.1083/jcb.127.6.1557

Grosse-Holz, F., Kelly, S., Blaskowski, S., Kaschani, F., Kaiser, M., & van der Hoorn, R. A. (2018). The transcriptome, extracellular proteome and active secretome of agroinfiltrated *Nicotiana*

benthamiana uncover a large, diverse protease repertoire. *Plant Biotechnology Journal, 16*(5), 1068–1084. https://doi.org/10.1111/pbi.12852

Gust, A. A., Pruitt, R., & Nürnberger, T. (2017). Sensing danger: Key to activating plant immunity. *Trends in Plant Science, 22*(9), 779–781. https://doi.org/10.1016/j.tplants.2017.07.005

Hander, T. (2016). *AtPeps as danger signals in Arabidopsis—their release from PROPEP proteins by highly specific metacaspases* [Doctoral dissertation, University of Basel]. https://edoc.unibas.ch/49099/

Hander, T., Fernández-Fernández, Á. D., Kumpf, R. P., Willems, P., Schatowitz, H., Rombaut, D., ... & Stael, S. (2019). Damage on plants activates Ca2+-dependent metacaspases for release of immunomodulatory peptides. *Science, 363*(6433), eaar7486. https://doi.org/10.1126/science.aar7486

Hou, S., Liu, D., & He, P. (2021). Phytocytokines function as immunological modulators of plant immunity. *Stress Biology, 1*, 1–14. https://doi.org/10.1007/s44154-021-00009-y

Hou, S., Liu, Z., Shen, H., & Wu, D. (2019a). Damage-associated molecular pattern-triggered immunity in plants. *Frontiers in Plant Science, 10*, 646. https://doi.org/10.3389/fpls.2019.00646

Hou, S., Shen, H., & Shao, H. (2019b). PAMP-induced peptide 1 cooperates with salicylic acid to regulate stomatal immunity in Arabidopsis thaliana. *Plant Signaling & Behavior, 14*(11), 1666657. https://doi.org/10.1080/15592324.2019.1666657

Huffaker, A., Pearce, G., & Ryan, C. A. (2006). An endogenous peptide signal in Arabidopsis activates components of the innate immune response. *Proceedings of the National Academy of Sciences, 103*(26), 10098–10103. https://doi.org/10.1073/pnas.0603727103

Huffaker, A., & Ryan, C. A. (2007). Endogenous peptide defense signals in Arabidopsis differentially amplify signaling for the innate immune response. *Proceedings of the National Academy of Sciences, 104*(25), 10732–10736. https://doi.org/10.1073/pnas.0703343104

Huh, S. U. (2022). Evolutionary diversity and function of metacaspases in plants: Similar to but not caspases. *International Journal of Molecular Sciences, 23*(9), 4588. https://doi.org/10.3390/ijms23094588

Jian, Y., Liu, Z., He, P., & Shan, L. (2024). An emerging connected view: Phytocytokines in regulating stomatal, apoplastic, and vascular immunity. *Current Opinion in Plant Biology, 82*, 102623. https://doi.org/10.1016/j.pbi.2024.102623

Jiang, Y., & Ding, P. (2023). Calcium signaling in plant immunity: A spatiotemporally controlled symphony. *Trends in Plant Science, 28*(1), 74–89. https://doi.org/10.1016/j.tplants.2022.11.001

Koenig, M., Moser, D., Leusner, J., Depotter, J. R., Doehlemann, G., & Misas Villamil, J. (2023). Maize phytocytokines modulate pro-survival host responses and pathogen resistance. *Molecular Plant-Microbe Interactions, 36*(9), 592–604. https://doi.org/10.1094/MPMI-01-23-0005-R

Koenig, M., Sorger, Z., Keh, S. P. Y., Doehlemann, G., & Misas Villamil, J. C. (2025). Quantitative detection of the maize phytocytokine Zip1 utilizing ELISA. *Journal of Experimental Botany, 76*(2), 299–311. https://doi.org/10.1093/jxb/erae423

Kourelis, J., Kaschani, F., Grosse-Holz, F. M., Homma, F., Kaiser, M., & van der Hoorn, R. A. L. (2019). A homology-guided, genome-based proteome for improved proteomics in the alloploid *Nicotiana benthamiana*. *BMC Genomics, 20*, 722. https://doi.org/10.1186/s12864-019-6058-6

Langmead, B., & Salzberg, S. L. (2012). Fast gapped-read alignment with Bowtie 2. *Nature Methods, 9*(4), 357–359. https://doi.org/10.1038/nmeth.1923

Liu, L., Liu, X., Bai, Z., Tanveer, M., Zhang, Y., Chen, W., ... & Huang, L. (2024). Small but powerful: RALF peptides in plant adaptive and developmental responses. *Plant Science*, 112085. https://doi.org/10.1016/j.plantsci.2024.112085

Liu, P., Shi, C., Liu, S., Lei, J., Lu, Q., Hu, H., ... & Yang, J. (2023). A papain-like cysteine protease-released small signal peptide confers wheat resistance to wheat yellow mosaic virus. Nature Communications, 14(1), 7773. https://doi.org/10.1038/s41467-023-43643-y

Liu, X. D., Hasan, M. M., & Fang, X. W. (2022). Phytocytokine SCREWs increase plant immunity through actively reopening stomata. *Journal of Plant Physiology, 279*, 153832. https://doi.org/10.1016/j.jplph.2022.153832

Liu, Z., Hou, S., Rodrigues, O., Wang, P., Luo, D., Munemasa, S., ... & Shan, L. (2022). Phytocytokine signalling reopens stomata in plant immunity and water loss. *Nature, 605*(7909), 332–339. https://doi.org/10.1038/s41586-022-04684-3

Luan, Q. L., Zhu, Y. X., Ma, S., Sun, Y., Liu, X. Y., Liu, M., ... & Wang, G. F. (2021). Maize metacaspases modulate the defense response mediated by the NLR protein Rp1-D21 likely by affecting its subcellular localization. *The Plant Journal, 105*(1), 151–166. https://doi.org/10.1111/tpj.15047

Luo, L. (2012). Plant cytokine or phytocytokine. *Plant Signaling & Behavior, 7*(12), 1513–1514. https://doi.org/10.4161/psb.22425

Ma, S., Shi, H., & Wang, G.-F. (2021). The potential roles of different metacaspases in maize defense response. *Plant Signaling & Behavior, 16*(6), 1909771. https://doi.org/10.1080/15592324.2021.1906574

Maddelein, D., Colaert, N., Buchanan, I., Hulstaert, N., Gevaert, K., & Martens, L. (2015). The iceLogo web server and SOAP service for determining protein consensus sequences. *Nucleic Acids Research, 43*(W1), W543–W546. https://doi.org/10.1093/nar/gkv385

Memon, A. R. (2004). The role of ADP-ribosylation factor and SAR1 in vesicular trafficking in plants. *Biochimica et Biophysica Acta (BBA) - Biomembranes, 1664*(1), 9–30. https://doi.org/10.1016/j.bbamem.2004.04.005

Misas Villamil, J. C., van der Hoorn, R. A. L., & Doehlemann, G. (2016). Papain-like cysteine proteases as hubs in plant immunity. *New Phytologist, 212*(4), 902–907. https://doi.org/10.1111/nph.14117

Misas Villamil, J. C., Mueller, A. N., Demir, F., Meyer, U., Ökmen, B., Schulze Hüynck, J., ... & Doehlemann, G. (2019). A fungal substrate mimicking molecule suppresses plant immunity via an inter-kingdom conserved motif. *Nature Communications, 10*, 1576. https://doi.org/10.1038/s41467-019-09472-8

Napier, R. M., Fowke, L. C., Hawes, C., Lewis, M., & Pelham, H. R. B. (1992). Immunological evidence that plants use both HDEL and KDEL for targeting proteins to the endoplasmic reticulum. *Journal of Cell Science, 102*(2), 261–271. https://doi.org/10.1242/jcs.102.2.261

Nebenfuhr, A., Ritzenthaler, C., & Robinson, D. G. (2002). Brefeldin A: Deciphering an enigmatic inhibitor of secretion. *Plant Physiology, 130*(3), 1102–1108. https://doi.org/10.1104/pp.011569

Niderman, T., Genetet, I., Bruyere, T., Gees, R., Stintzi, A., Legrand, M., ... & Mosinger, E. (1995). Pathogenesis-related PR-1 proteins are antifungal: Isolation and characterization of three 14-kilodalton proteins of tomato and of a basic PR-1 of tobacco with inhibitory activity against *Phytophthora infestans*. *Plant Physiology, 108*(1), 17–27. https://doi.org/10.1104/pp.108.1.17

Pearce, G., Strydom, D., Johnson, S., & Ryan, C. A. (1991). A polypeptide from tomato leaves induces wound-inducible proteinase inhibitor proteins. *Science, 253*(5022), 895–897. https://doi.org/10.1126/science.253.5022.895

Rhodes, J., Yang, H., Moussu, S., Boutrot, F., Santiago, J., & Zipfel, C. (2021). Perception of a divergent family of phytocytokines by the Arabidopsis receptor kinase MIK2. *Nature Communications, 12*(1), 705. https://doi.org/10.1038/s41467-021-20932-y

Robinson, D. G., Albrecht, S., & Moriysu, Y. (2004). The V-ATPase inhibitors concanamycin A and bafilomycin A lead to Golgi swelling in tobacco BY-2 cells. *Protoplasma, 224*(3–4), 255–260. https://doi.org/10.1007/S00709-004-0070-6

Ryan, C. A. (2000). The systemin signaling pathway: Differential activation of plant defensive genes. *Biochimica et Biophysica Acta (BBA) - Protein Structure and Molecular Enzymology, 1477*(1–2), 112–121. https://doi.org/10.1016/S0167-4838(99)00269-1

Rzemieniewski, J., & Stegmann, M. (2022). Regulation of pattern-triggered immunity and growth by phytocytokines. *Current Opinion in Plant Biology, 68*, 102230. https://doi.org/10.1016/j.pbi.2022.102230

Sauter, M. (2015). Phytosulfokine peptide signalling. *Journal of Experimental Botany, 66*(17), 5161–5169. https://doi.org/10.1093/jxb/erv071

Schardon, K., Hohl, M., Graff, L., Pfannstiel, J., Schulze, W., Stintzi, A., & Schaller, A. (2016). Precursor processing for plant peptide hormone maturation by subtilisin-like serine proteinases. *Science, 354*(6319), 1594–1597. https://doi.org/10.1126/science.aai8550

Segonzac, C., & Monaghan, J. (2019). Modulation of plant innate immune signaling by small peptides. *Current Opinion in Plant Biology, 51*, 22–28. https://doi.org/10.1016/j.pbi.2019.03.007

Shen, X., Stührwohldt, N., & Lin, C. (2023). The research process of PSK biosynthesis, signaling transduction, and potential applications in *Brassica napus*. *Plants, 12*(17), 3075. https://doi.org/10.3390/plants12173075

Soh, W. T., Demir, F., Dall, E., Perrar, A., Dahms, S. O., Kuppusamy, M., Brandstetter, H., & Huesgen, P. F. (2020). ExteNDing proteome coverage with legumain as a highly specific digestion protease. *Analytical Chemistry, 92*(4), 2961–2971. https://doi.org/10.1021/acs.analchem.9b03604

Srivastava, R., Liu, J. X., Guo, H., Yin, Y., & Howell, S. H. (2009). Regulation and processing of a plant peptide hormone, AtRALF23, in Arabidopsis. *The Plant Journal, 59*(6), 930–939. https://doi.org/10.1111/j.1365-313X.2009.03926.x

Srivastava, R., Liu, J. X., & Howell, S. H. (2008). Proteolytic processing of a precursor protein for a growth-promoting peptide by a subtilisin serine protease in *Arabidopsis*. *The Plant Journal, 56*(2), 219–227. https://doi.org/10.1111/j.1365-313X.2008.03598.x

Stael, S., Miller, L. P., Fernandez-Fernandez, A. D., & Van Breusegem, F. (2022). Detection of damage-activated metacaspase activity by western blot in plants. In *Plant proteases and plant cell death: Methods and protocols* (pp. 127–137). New York, NY: Springer US. https://doi.org/10.1007/978-1-0716-2079-3_11

Stael, S., Sabljić, I., Audenaert, D., Andersson, T., Tsiatsiani, L., Kumpf, R. P., Vidal-Albalat, A., Lindgren, C., Vercammen, D., Jacques, S., Nguyen, L., Njo, M., Fernández-Fernández, Á. D., Beunens, T., Timmerman, E., Gevaert, K., Van Montagu, M., Ståhlberg, J., Bozhkov, P. V., Linusson, A., Beeckman, T., & Van Breusegem, F. (2023). Structure–function study of a Ca^{2+}-independent metacaspase involved in lateral root emergence. *Proceedings of the National Academy of Sciences of the United States of America, 120*(22), e2303480120. https://doi.org/10.1073/pnas.2303480120

Štrancar, V., van Midden, K. P., Krahn, D., Morimoto, K., Novinec, M., Funk, C., ... & van der Hoorn, R. A. (2022). Activity-based probes trap early active intermediates during metacaspase activation. *iScience, 25*(11), 105399. https://doi.org/10.1016/j.isci.2022.105247

Stührwohldt, N., Bühler, E., Sauter, M., & Schaller, A. (2021). Phytosulfokine (PSK) precursor processing by subtilase SBT3.8 and PSK signaling improve drought stress tolerance in *Arabidopsis*. *Journal of Experimental Botany, 72*(9), 3427–3440. https://doi.org/10.1093/jxb/erab017

Stührwohldt, N., Scholl, S., Lang, L., Katzenberger, J., Schumacher, K., & Schaller, A. (2020). The biogenesis of CLEL peptides involves several processing events in consecutive compartments of the secretory pathway. *eLife, 9*, e55580. https://doi.org/10.7554/eLife.55580

Sueldo, D., Ahmed, A., Misas-Villamil, J., Colby, T., Tameling, W., Joosten, M. H., & van der Hoorn, R. A. (2014). Dynamic hydrolase activities precede hypersensitive tissue collapse in tomato seedlings. *New Phytologist, 203*(3), 913–925.

Sweet, R. M., & Eisenberg, D. (1983). Correlation of sequence hydrophobicities measures similarity in three-dimensional protein structure. *Journal of Molecular Biology, 171*(4), 479–488. https://doi.org/10.1016/S0022-2836(83)80016-6

Takáč, T., Pechan, T., Šamajová, O., Ovečka, M., Richter, H., Eck, C., Niehaus, K., & Šamaj, J. (2012). Wortmannin treatment induces changes in *Arabidopsis* root proteome and post-Golgi compartments. *Journal of Proteome Research, 11*(6), 3127–3142. https://doi.org/10.1021/PR201111N

Tanaka, K., & Heil, M. (2021). Damage-associated molecular patterns (DAMPs) in plant innate immunity: Applying the danger model and evolutionary perspectives. *Annual Review of Phytopathology, 59*, 53–75. https://doi.org/10.1146/annurev-phyto-082718-100146

Tost, A. S., Kristensen, A., Olsen, L. I., Axelsen, K. B., & Fuglsang, A. T. (2021). The PSY peptide family—Expression, modification and physiological implications. *Genes, 12*(2), 218. https://doi.org/10.3390/genes12020218

Tsiatsiani, L., Timmerman, E., De Bock, P. J., Vercammen, D., Stael, S., Van De Cotte, B., ... & Van Breusegem, F. (2013). The Arabidopsis metacaspase9 degradome. The Plant Cell, 25(8), 2831–2847. https://doi.org/10.1105/tpc.113.115287

Tyanova, S., Temu, T., & Cox, J. (2016). The MaxQuant computational platform for mass spectrometry-based shotgun proteomics. *Nature Protocols, 11*(12), 2301–2319. https://doi.org/10.1038/nprot.2016.136

van der Linde, K., Hemetsberger, C., Kastner, C., Kaschani, F., van der Hoorn, R. A., Kumlehn, J., & Doehlemann, G. (2012a). A maize cystatin suppresses host immunity by inhibiting apoplastic cysteine proteases. *The Plant Cell, 24*(3), 1285–1300. https://doi.org/10.1105/tpc.111.093732

Vercammen, D., Van De Cotte, B., De Jaeger, G., Eeckhout, D., Casteels, P., Vandepoele, K., ... & Van Breusegem, F. (2004). Type II metacaspases Atmc4 and Atmc9 of Arabidopsis thaliana cleave substrates after arginine and lysine. *Journal of Biological Chemistry*, 279(44), 45329–45336. https://doi.org/10.1126/science.aar7486

Wang, C., & Luan, S. (2024). Calcium homeostasis and signaling in plant immunity. *Current Opinion in Plant Biology, 77*, 102485. https://doi.org/10.1016/j.pbi.2023.102485

Wang, J., Ding, Y., Wang, J., Hillmer, S., Miao, Y., Lo, S. W., ... & Jiang, L. (2010). EXPO, an exocyst-positive organelle distinct from multivesicular endosomes and autophagosomes, mediates cytosol to cell wall exocytosis in Arabidopsis and tobacco cells. *The Plant Cell, 22*(12), 4009–4030. https://doi.org/10.1105/tpc.110.080697

Wang, L., Albert, M., Einig, E., Fürst, U., Krust, D., & Felix, G. (2018). The systemin receptor SYR1 enhances resistance of tomato against herbivorous insects. *Nature Plants, 4*(3), 152–156. https://doi.org/10.1038/s41477-018-0106-0

Wrzaczek, M., Vainonen, J. P., Stael, S., Tsiatsiani, L., Help-Rinta-Rahko, H., Gauthier, A., ... & Kangasjärvi, J. (2015). GRIM REAPER peptide binds to receptor kinase PRK5 to trigger cell death in Arabidopsis. *The EMBO Journal, 34*(1), 55–66. https://doi.org/10.15252/embj.201488582

Xu, F., & Copeland, C. (2012). Nuclear extraction from Arabidopsis thaliana. *Bio-protocol, 2*(24), e306. https://doi.org/10.21769/BioProtoc.306

Yamaguchi, K., & Kawasaki, T. (2021). Pathogen- and plant-derived peptides trigger plant immunity. *Peptides, 144*, 170611. https://doi.org/10.1016/j.peptides.2021.170611

Zelman, A. K., & Berkowitz, G. A. (2023). Plant elicitor peptide (Pep) signaling and pathogen defense in tomato. *Plants, 12*(15), 2856. https://doi.org/10.3390/plants12152856

Zhao, Y., & Li, S. (2017). Isolation of cytosol, microsome, free polysomes (FPs) and membrane-bound polysomes (MBPs) from Arabidopsis seedlings. *Bio-protocol, 7*(15), e2436. https://doi.org/10.21769/BioProtoc.2436

Zhu, P., Yu, X. H., Wang, C., Zhang, Q., Liu, W., McSweeney, S., ... & Liu, Q. (2020). Structural basis for Ca2+-dependent activation of a plant metacaspase. *Nature Communications, 11*(1), 2249. https://doi.org/10.1038/s41467-020-15830-8

Ziemann, S., van der Linde, K., Lahrmann, U., Acar, B., Kaschani, F., Colby, T., ... & Doehlemann, G. (2018). An apoplastic peptide activates salicylic acid signalling in maize. *Nature Plants, 4*(3), 172–180. https://doi.org/10.1038/s41477-018-0116-y

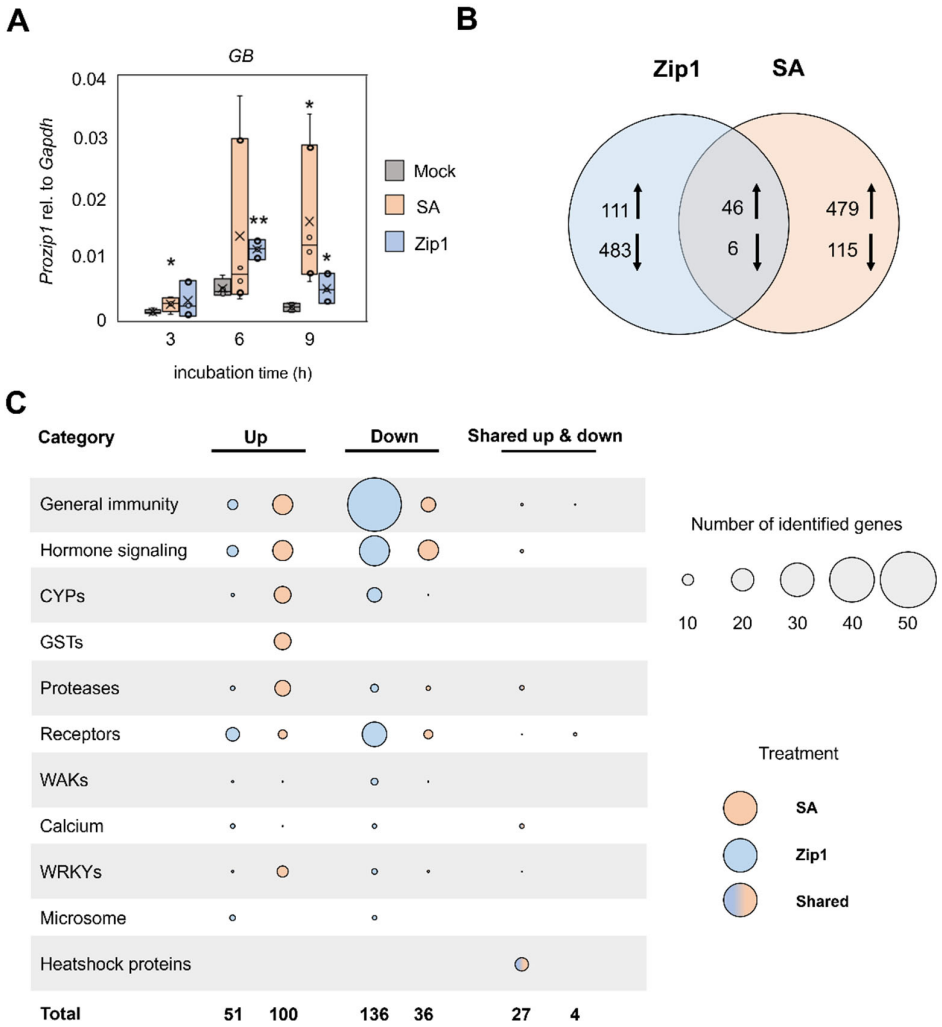

Figure 1. Zip1 treatment induces *Prozip1* and triggers transcriptional responses distinct from SA. (A) *Prozip1* expression after SA and Zip1 treatments. Leaves of 8 days old maize seedlings cv. Golden Bantam (GB) were treated with 2 mM SA, 5 µM Zip1 or water (mock). Samples were collected at 3, 6, 9 hours after treatment (hpi) and *Prozip1* gene expression was analyzed by qRT-PCR. *Prozip1* expression was normalized to *ZmGapdh*. **(B)** Differential gene expression 6 hpi after SA and Zip1 treatment. The Venn diagram shows the number of common and differentially expressed genes (DEGs) found in SA and Zip1 treatment normalized to the mock control. Arrows represent the number of upregulated (↑) or downregulated (↓) genes. **(C)** Gene ontology of selected DEGs present in SA and Zip1 treatment. DEGs found in SA and Zip1 were grouped based on their gene function (geneontology.org). Immune- and defense-related DEGs of the total DEGs are depicted as distinct categories. Circle sizes reflect the number of DEGs found in the particular group (e.g., 0.4 cm = 10 DEGs). Depicted are up-, and down-regulated genes of treatment specific and shared DEGs (present in both SA and Zip1 = shared). SA (red), Zip1 (blue) and shared (red/blue). GSTs = glutathione-S-transferases, CYPs = cytochrome P450s, WAKs = wall-associated receptor kinases, WRKY = group of transcription factors (TF) involved in stress/defense

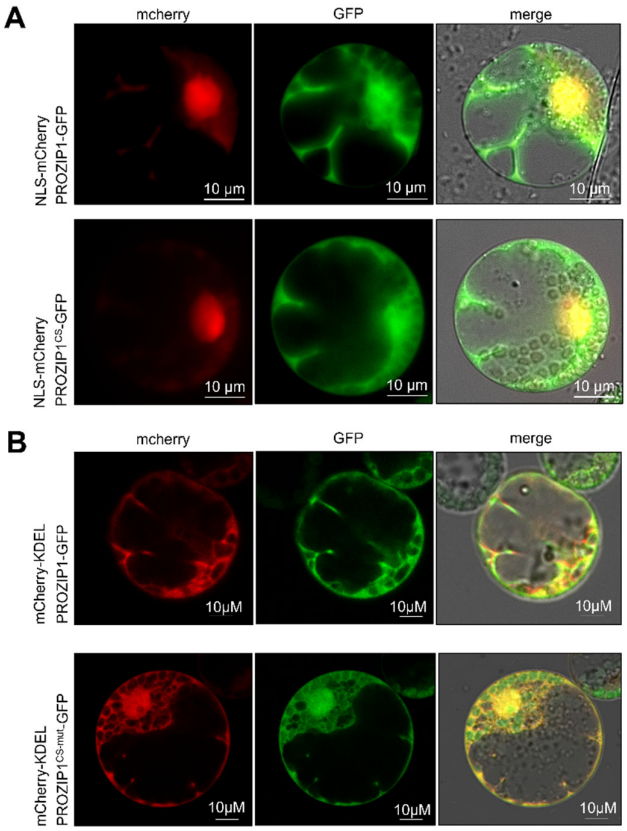

Figure 2. PROZIP1 localizes intracellularly to cytosol and ER. (A) Fluorescence microscopy of PROZIP1-GFP and PROZIP1^{CSmut}-GFP. PROZIP1-GFP and its cleavage site mutant (PROZIP1^{CSmut}-GFP) were co-expressed with a nuclear localized mCherry (NLS-mCherry) in maize protoplast. Co-localization was analyzed 16h post transfection by fluorescence microscopy. **(B)** Confocal microscopy of PROZIP1-GFP and PROZIP1^{CSmut}-GFP. PROZIP1-GFP and PROZIP1$^{CS\text{-}mut}$-GFP were co-expressed with mCherry-KDEL in maize protoplast. Co-localization was analyzed 16h post transfection by confocal microscopy. All experiments were conducted in at least three different and independent biological replicates.

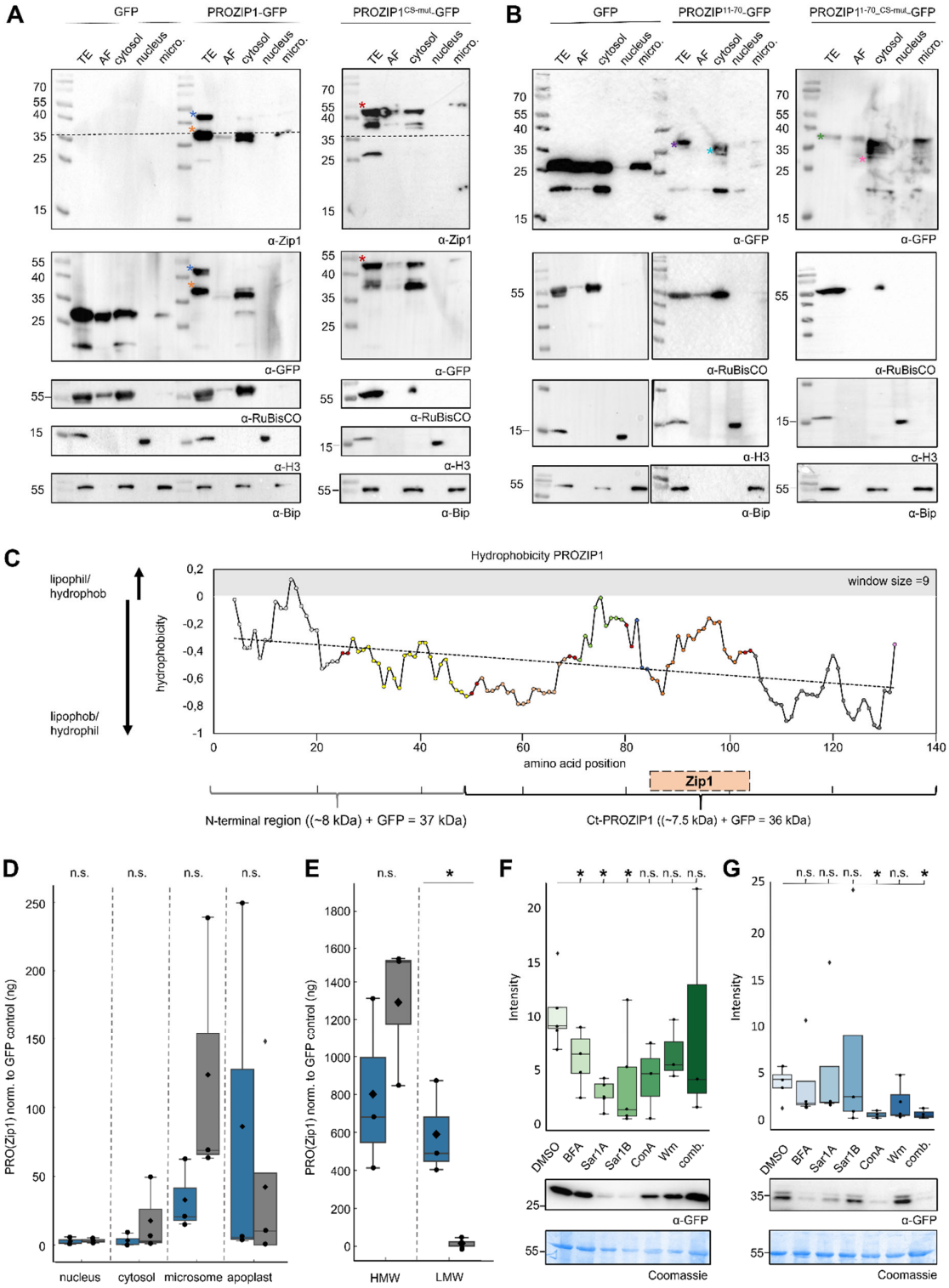

Figure 3. N-terminal processing of PROZIP1 facilitates C-terminal translocation to the apoplast (A) Western blots of PROZIP1-GFP and PROZIP1$^{CS\text{-}mut}$-GFP that were transiently overexpressed in *N. benthamiana* and samples were tested for cell compartment analyses at 3 dpi. Cell markers as controls of fractionation: cytosol (RuBisCO), nucleus (Histon H3), microsome (Bip). PROZIP1-GFP (blue asterisk), a cleavage product of PROZIP1-GFP (orange asterisk) and PROZIP1$^{CS\text{-}mut}$-GFP (red asterisk) are labeled. Dashed line highlights differences in prominent cleavage products of PROZIP1-GFP and PROZIP1$^{CS\text{-}mut}$-GFP. Total

protein extracts (TE), apoplastic fluid (AF), microsome (micro.) **(B)** Western blot of N-terminal PROZIP1 (PROZIP$^{11-70}$) and PROZIP1^{CS-mut} (PROZIP1$^{CS-mut1-70}$); fused to GFP and transiently overexpressed in *N. benthamiana*. The experiment was conducted and setup like described before in A. Full length PROZIP1$^{1-70}$-GFP (purple asterisk), PROZIP1$^{1-70_CSmut}$-GFP (cyan asterisk) are marked. **(C)** The amino acid sequence of PROZIP1 was used for a hydropathy plot based on Sweet and Eisenberg (1983). The x-axis shows the hydropathy index and the y-axis the amino acid residues present in PROZIP1. The dashed line is the regression curve. The position of the N-terminal region of PROZIP1 and the Zip1-containing Ct-PROZIP1 with corresponding sizes is shown. **(D)** Subcellular fractions were subjected to an ELISA-based assay and tested for the presence of Zip1-containing fragments using the α-Zip1 antibody (Koenig *et al*., 2025). PROZIP1-GFP (blue) and PROZIP1^{CS-mut}-GFP (grey) are labeled. Signals were normalized to the GFP-background. Independent biological replicates are represented by dots. The mean is represented as diamond inside boxplots, outliers are shown outside of boxplots. Students t-test was performed to test for significance (p=0.05). **(E)** Infiltrated leaves of *N. benthamiana* transiently overexpressing PROZIP1-GFP and PROZIP1^{CS-mut}-GFP was isolated and filtrated (>5kDa cut off) to generate high- and low molecular weight fractions (HMW vs. LMW). HMW- and LMW were subjected to an ELISA and the amount of Zip1 was quantified (Koenig *et al*., 2025). PROZIP1-GFP (blue) and PROZIP1^{CS-mut}-GFP (grey) are labeled. Signals were normalized to the GFP control. Independent biological replicates are represented by dots. The mean is represented as diamond inside boxplots. Students t-test was performed to test for significance (p=0.05). **(F)** Quantification of Western Blot signals of apoplastic Ct-PROZIP1-GFP in presence and absence of secretory inhibitors. *N. benthamiana* leaves were pre-treated with 10 µg/ml brefeldin A (BFA), 0.5µM Concanamycin A (ConA), 35µM Wortmannin (Wm) or a combination of BFA, ConA and Wm (comb.) for 4h prior *Agrobacterium*-mediated overexpression of PROZIP1-GFP. Additionally, Sar1A and Sar1B, small GTPases involved in ER-Golgi vesicular trafficking, were co-expressed. Apoplastic fluid was isolated at 2 dpi. spNtPR1-GFP (green) served as control. Ct-PROZIP1-GFP (blue, 36 kDa) signals from at least three independent biological replicates were quantified from the anti-GFP blots, normalized to total protein content and values were plotted. Independent biological replicates are represented by dots. Students t-test was performed to test for significance (p=0.05). Depicted is the standard error of the mean (SEM); shown is a representative blot.

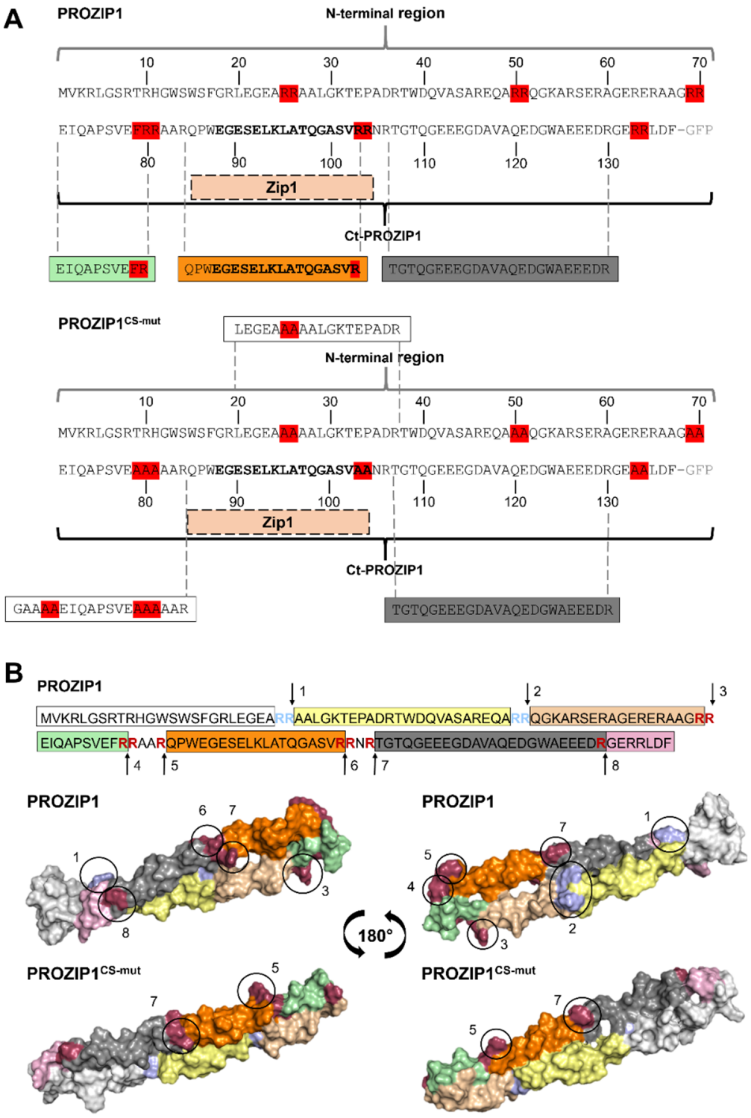

Figure 4. Arginine-dependent processing of PROZIP1. (A) N-termini generated from PROZIP1-GFP and PROZIP1$^{CS\text{-}mut}$-GFP detected by ATOMS. Maize protoplasts were transfected with PROZIP1-GFP or PROZIP1$^{CS\text{-}mut}$-GFP and samples were harvested after 16 hours to perform a GFP pull-down. Newly generated peptide N-termini were marked by reductive demethylation and identified by mass spectrometry. The identified labeled peptides (sequences in black framed boxes) are shown at the corresponding amino acid position of PROZIP1 or PROZIP1$^{CS\text{-}mut}$ sequence. Zip1 sequence is shown in bold. Arg (R) to Ala (A) mutations between PROZIP1 and PROZIP1$^{CS\text{-}mut}$ are highlighted in red. **(B)** Predicted 3D structure of PROZIP1. The amino acid sequence of PROZIP1 (top) and a surface model prediction of PROZIP1 and PROZIP1$^{CS\text{-}mut}$ (bottom left) are shown. Both models were rotated in 180° angle (bottom right). Peptides and cleavage fragments identified in the HUNTER were colored in the sequence and in the models. Zip1 sequence is depicted in orange. Putative cleavage sites predicted by the Western blot analysis are shown in light blue, while those identified by MS are depicted in dark red. Arrows represent the identified cleavage sites and are numbered from the N- to the C-terminal part of the sequence. Numbers and circles in the corresponding models represent the potential cleavage sites marked by the arrows. Models were generated by I-TASSER and visualized by PyMOL. C-scores of selected models were -4.39 (PROZIP1) to -4.21 (PROZIP1$^{CS\text{-}mut}$) being close to -5 as the best possible score while 2 is the worst.

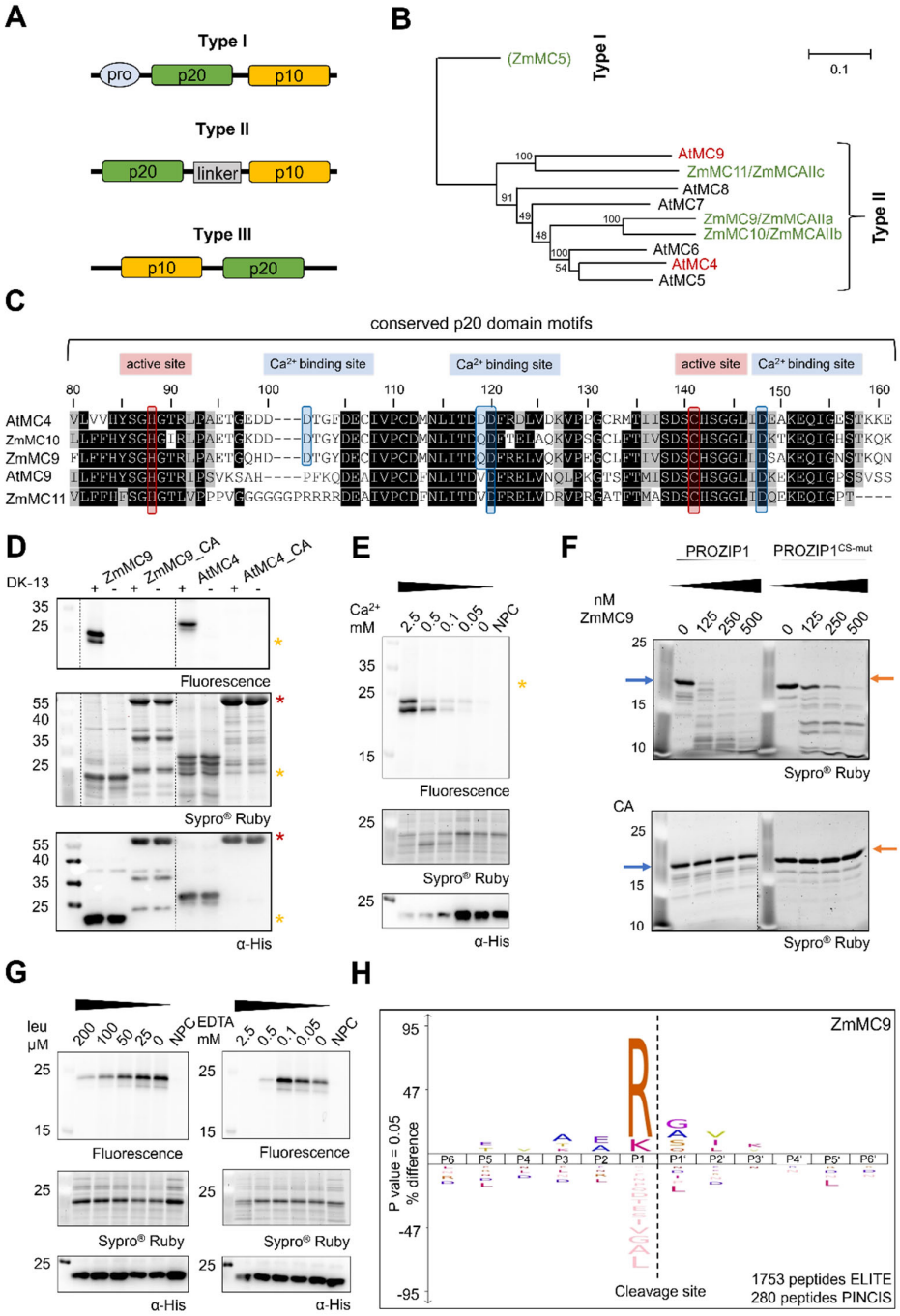

Figure 5. The Ca^{2+}-dependent metacaspase ZmMC9 cleaves PROZIP1 in an arginine-dependent manner. (A) Schematic illustration of the domain structure of plant metacaspases. There are three types of plant metacaspases, all consisting of a p20 domain (green) harboring the enzymes active site and a p10 domain (yellow). Type I metacaspases are produced as inactive forms (zymogens) and contain a pro-domain (blue) that is removed for activation. Type II metacaspases have a linker domain between the p20 and the p10 (grey) domain. Type III metacaspases have an inverted p20 and p10 domain and do not have a linker nor a pro-domain. **(B)** Amino acid sequences of Arabidopsis and maize metacaspases were phylogenetic analyzed by Luan *et al.*, 2021 and a modified overview of the type II metacaspases is shown. Maize metacaspases are depicted in green. AtMC4 and AtMC9 are highlighted in red as they have been identified in phytocytokine release. **(C)** Sequences of

Arabidopsis AtMC4, AtMC9 and maize ZmMC9, ZmMC10 and ZmMC11 metacaspases were aligned using ClustalW and BioEdit to identify putative Ca^{2+}-binding sites (blue) and the protease active site (red). Numbers represent the amino acid position of AtMC4 **(D)** ABPP, SYPRO® Ruby and α-His blot of ZmMC9, AtMC4 and their respective inactive mutants (AtMC4_CA and ZmMC9_CA). ZmMC9, AtMC4 and active site mutants were heterologous expressed in *E. coli* and their activity was monitored using an activity-based protein profiling (ABPP) using the probe DK-13 (Strancar *et al*., 2022). AtMC4 and its inactive mutant served as controls. Sypro® Ruby was used as loading control. An anti-His blot was performed to show the presence of the heterologous expressed proteins as proteases are His-tagged. Red asterisks indicate full-length proteins of ZmMC9_CA and AtMC4_CA. Yellow asterisks show p20 domains of ZmMC9 and AtMC4. **(E)** ABPP of ZmMC9 at different Ca^{2+} concentrations. A $CaCl_2$ concentration range (0 to 2.5 mM) was performed to assess the Ca^{2+}-dependent activity of ZmMC9. ZmMC9 activity was monitored using the probe DK-13 (Strancar *et al*., 2022). 285 µM of ZmMC9 were used for each reaction. Sypro® Ruby staining and anti-His blots were used to visualize the presence of ZmMC9. NPC=No Probe Control. (**F)** Coincubation of different ZmMC9 concentrations with PROZIP1 and $PROZIP1^{CS\text{-}mut}$. A PROZIP1 and $PROZIP1^{CS\text{-}mut}$ stability experiment was performed in a concentration range (0 to 500 nM) of ZmMC9 and ZmMC9_CA. Samples were incubated for 30 min and signals were monitored using Sypro® Ruby. **(G)** Activity of ZmMC9 in presence of leupeptin and EDTA. ZmMC9 was pre-incubated with leupeptin or EDTA for 30 min followed by ABPP labelling using DK-13 (Strancar *et al*., 2022). Samples were analyzed by fluorescent scanning and Sypro® Ruby was used as loading control. **(I)** PICS of ZmMC9. Proteomic identification of cleavage sites (PICS) was performed using ZmMC9. 22.5 µM of ZmMC9 and ZmMC9_CA were incubated with 40 µg legumain library for 1h at room temperature. Incubation was stopped with a mix of 100 µM leupeptin and 10 mM EDTA before MS analyzes.

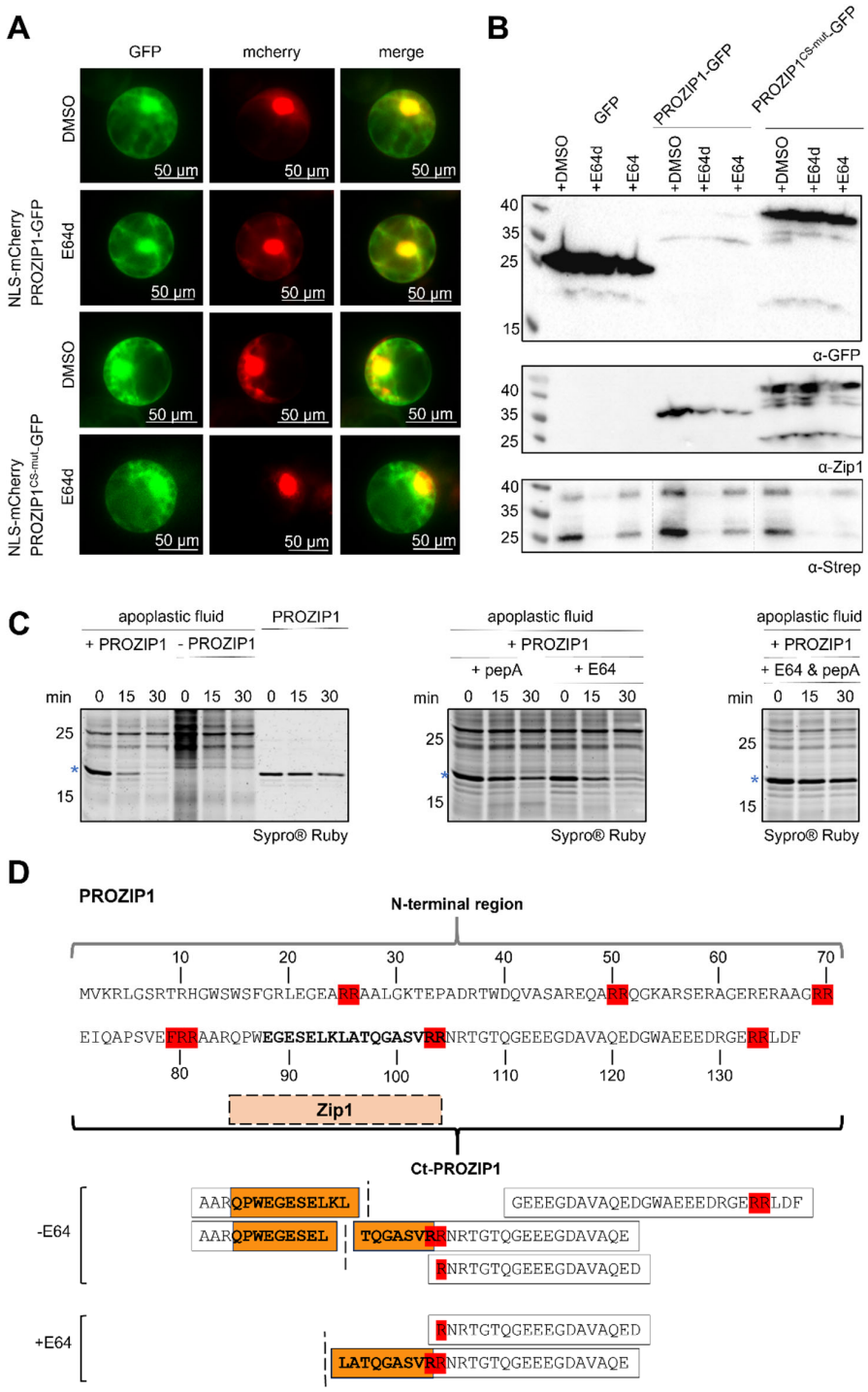

Figure 6. Apoplastic PLCPs cleave and clear PROZIP1/Zip1 in the apoplast. (A) Fluorescence microscopy of PROZIP1-GFP and PROZIP1$^{CS\text{-}mut}$-GFP in presence of E64d. PROZIP1-GFP and PROZIP1$^{CS\text{-}mut}$-GFP were co-expressed with NLS-mCherry in maize protoplast. Protoplasts were treated with 30µM of the cell-permeable PLCP inhibitor E64d or DMSO. Samples were analyzed 16h post transfection. **B)** Western blots and ABPP of PROZIP1-GFP and PROZIP1$^{CS\text{-}mut}$-GFP in presence of E64d. Protein extracts obtained from (A) and E64 treated extracts were used for Western blot using the α-Zip1 and α-GFP antibody. In addition, an ABPP was performed using DCG04-biotin to determine PLCP activity, which was visualized by Western blot using the streptavidin antibody (Greenbaum *et al*., 2000). **(C)** Coincubation of apoplastic fluid with PROZIP1. Maize plants were treated with 2mM SA to

activate PLCPs and apoplastic fluid was obtained 24 hours post infiltration. Recombinant PROZIP1 was co-incubated with apoplastic fluid and cleavage of PROZIP1 was monitored over time. In addition, 30µM of E64 and/or aspartic protease inhibitor pepA were added. Cleavage activity was monitored by Sypro® Ruby staining. Recombinant PROZIP1 without apoplastic fluid served as the control. **(D)** N-termini generated from recombinant PROZIP1 detected by ATOMS. Apoplastic fluid of SA-treated maize plants was fractionated by anion exchange chromatography (IEC) and a fraction known to be enriched in PLCPs was collected (Misas Villamil *et al*., 2019). The PLCP-enriched fraction known to contain active CP1 and CP2 was pre-incubated with pepA, EDTA and DCI and presence/absence of E64 prior the incubation with recombinant PROZIP1. Primary amines were demethylated and peptides identified by mass spectrometry. The position of Zip1 within in PROZIP1 is indicated by the light orange box. Zip1 or parts of Zip1 were highlighted by orange within the identified peptides.

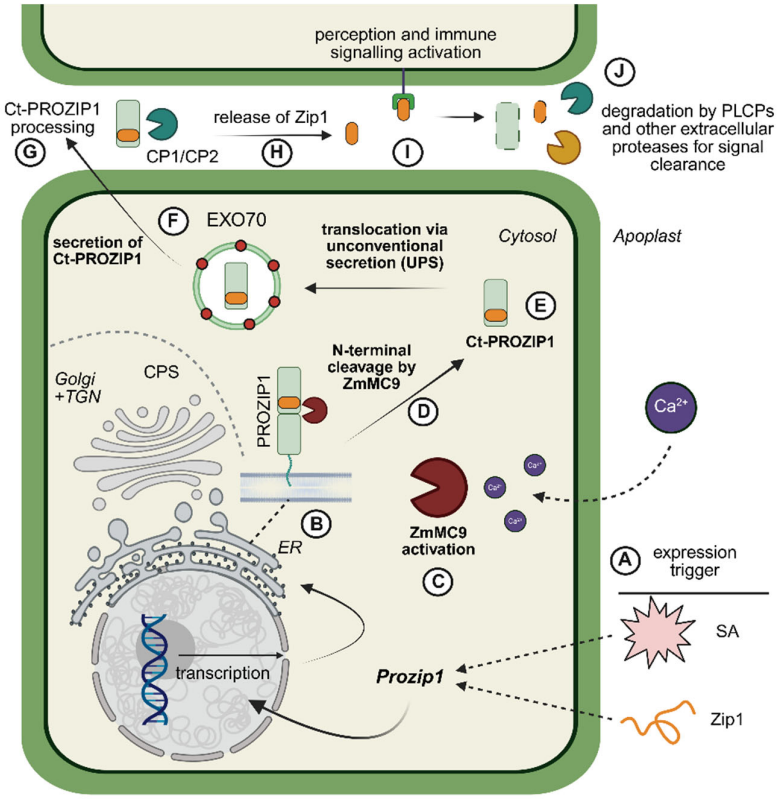

Figure 7. Mechanism for phytocytokine maturation, activation, and clearance of Zip1. SA and Zip1 peptide are inducers of *Prozip1* expression **(A)** Post translation PROZIP1 is attached N-terminally to the ER membrane **(B)**. Activation of calcium-dependent metacaspase ZmMC9 **(C)** is required to release PROZIP1 from the ER **(D)** and for N-terminal cleavage of PROZIP1 to release Ct-PROZIP1 **(E)**. Translocation of Ct-PROZIP1 **(F)** via unconventional protein secretion (UPS) likely involves EXPO (EXO70) or UPS associated vesicles, but not the conventional protein secretion (CPS) pathway involving Golgi and trans-Golgi-network (TGN). In the apoplast, PLCPs, including CP1 and CP2 process Ct-PROZIP1 **(G)** to release Zip1 (orange) **(H)** that is perceived by a yet undescribed receptor to elicit immune signaling **(I)**. Excess extracellular Zip1 and Ct-PROZIP1 are degraded by a cocktail of apoplastic proteases including PLCPs, making the release and perception of Zip1 a time- and concentration-dependent process **(J)**.